Medical Physics
The International Journal of Medical Physics Research and Practice

Accelerator beam data commissioning equipment and procedures: Report of the TG-106 of the Therapy Physics Committee of the AAPM

Indra J. Das, Chee-Wai Cheng, Ronald J. Watts, Anders Ahnesjö, John Gibbons, X. Allen Li, Jessica Lowenstein, Raj K. Mitra, William E. Simon, and Timothy C. Zhu

Citation: Medical Physics **35**, 4186 (2008); doi: 10.1118/1.2969070
View online: http://dx.doi.org/10.1118/1.2969070
View Table of Contents: http://scitation.aip.org/content/aapm/journal/medphys/35/9?ver=pdfcov
Published by the American Association of Physicists in Medicine

Accelerator beam data commissioning equipment and procedures: Report of the TG-106 of the Therapy Physics Committee of the AAPM

Indra J. Das[a)]
Department of Radiation Oncology, University of Pennsylvania, Philadelphia, Pennsylvania 19104

Chee-Wai Cheng
Department of Radiation Oncology, Morristown Memorial Hospital, Morristown, New Jersey 07962

Ronald J. Watts
International Medical Physics Services, San Antonio, Texas 78232

Anders Ahnesjö
Uppsala University and Nucletron Scandinavia AB, 751 47 Uppsala, Sweden

John Gibbons
Department of Radiation Oncology, Mary Bird Perkins Cancer Center, Baton Rouge, Louisiana 70809

X. Allen Li
Department of Radiation Oncology, Medical College of Wisconsin, Milwaukee, Wisconsin 53226

Jessica Lowenstein
Radiological Physics Center, MD Anderson Cancer Center, Houston, Texas 77030

Raj K. Mitra
Department of Radiation Oncology, Ochsner Clinic, New Orleans, Louisiana 70121

William E. Simon
Sun Nuclear Corporation, Melbourne, Florida 32940

Timothy C. Zhu
Department of Radiation Oncology, University of Pennsylvania, Philadelphia, Pennsylvania 19104

(Received 4 February 2008; revised 18 July 2008; accepted for publication 18 July 2008; published 22 August 2008)

For commissioning a linear accelerator for clinical use, medical physicists are faced with many challenges including the need for precision, a variety of testing methods, data validation, the lack of standards, and time constraints. Since commissioning beam data are treated as a reference and ultimately used by treatment planning systems, it is vitally important that the collected data are of the highest quality to avoid dosimetric and patient treatment errors that may subsequently lead to a poor radiation outcome. Beam data commissioning should be performed with appropriate knowledge and proper tools and should be independent of the person collecting the data. To achieve this goal, Task Group 106 (TG-106) of the Therapy Physics Committee of the American Association of Physicists in Medicine was formed to review the practical aspects as well as the physics of linear accelerator commissioning. The report provides guidelines and recommendations on the proper selection of phantoms and detectors, setting up of a phantom for data acquisition (both scanning and no-scanning data), procedures for acquiring specific photon and electron beam parameters and methods to reduce measurement errors ($<1\%$), beam data processing and detector size convolution for accurate profiles. The TG-106 also provides a brief discussion on the emerging trend in Monte Carlo simulation techniques in photon and electron beam commissioning. The procedures described in this report should assist a qualified medical physicist in either measuring a complete set of beam data, or in verifying a subset of data before initial use or for periodic quality assurance measurements. By combining practical experience with theoretical discussion, this document sets a new standard for beam data commissioning.
[DOI: 10.1118/1.2969070]

Key words: accelerator, commissioning, data acquisition

TABLE OF CONTENTS

I. INTRODUCTION

I.A. Purpose

Beam data commissioning should be independent of individuals collecting the data and scanning systems if it is performed with appropriate knowledge and proper tools. Data variation among beam collectors should be as minimal as possible ($<1\%$). To achieve this goal, this report has been prepared to facilitate accelerator beam data commissioning by describing specific setup and measurement techniques, reviewing different types of radiation phantoms and detectors, discussing possible sources of error, and recommending procedures for acquiring specific photon and electron beam parameters.

I.B. Background

I.B.1. Need for commissioning data

Radiation treatment outcome is directly related to the accuracy in the delivered dose to the patient that is dependent on the accuracy of beam data used in the treatment planning process. These data are obtained during the initial commissioning of the linear accelerator and are treated as the standard data for clinical use and should be verified periodically as described by TG-40 (Ref. 1) by a qualified medical physicist to ensure that machine parameters have not changed during normal operation. For any substantial changes in a treatment planning system (TPS), for example, change in dose algorithm, additional commissioning data may be warranted based on the TPS requirements.[2]

As the manufacturing processes for linear accelerators have significantly matured, there has been an attempt by vendors to standardize machines to have identical beam characteristics. In some cases, "golden" beam data sets are provided which contain most or all of the commissioning beam data required by the TPS. If the same vendor provided the TPS, the golden beam data may already be input into the

computer. In such cases, users have the choice of measuring all the required data, or verifying a carefully selected subset of the data at time of beam commissioning. The preferred option will depend on a number of factors, such as the make and model of the accelerator and TPS, and the accuracy required for clinical use.

The following concerns should be carefully evaluated before the use of any golden beam data within a clinic. First, it is not evident that manufacturing procedures for all linear accelerators have produced a level of reproducibility acceptable for clinical use. For example, variations in beam parameters have been noted between beams with the same nominal energies.[3–5] Second, on-site changes made during installation and acceptance of the user's accelerator (e.g., changes in beam energy and/or profiles from beam steering) will not be modeled in the golden data. Third, the beam characteristics of the soft wedges are made by moving jaws that depend on the speed parameters of the jaws and a deviation at site could affect the beam profile of the soft wedge. Fourth, although acceptable agreement with the golden data set may be found in individual checks, it may be that some clinical setups will have multiple errors, which combine to produce unacceptable results. Finally, the commissioned beam data also provide a thorough check of the accelerator, which may uncover problems that may not otherwise be discovered with a mere spot check.

At a minimum, however, a golden beam dataset is an excellent source of quality assurance for verifying the user's commissioning results. These data along with those available from the Radiological Physics Center at MD Anderson Cancer Center[6–8] can be used to ensure that the user's beam data are in reasonably good agreement with those from other institutions. Monte Carlo simulation could also provide good standard data. However, measurements are still required as benchmarks for validation of any Monte Carlo[9–13] simulation.

It is beyond the scope of this report to make any specific recommendations as to what measurements are required at the time of beam commissioning of a linear accelerator. However, at a minimum, the following data should be collected during commissioning:

- For photon beams—percent depth dose (PDD) and profiles (in-plane and/or cross-plane) at various depths for open and wedge fields, data related to multileaf collimator (MLC) such as inter- and intraleaf leakage, penumbra, tongue and grove effect, etc., head (collimator) scatter, total scatter, tray, and wedge factors.
- For electron beams—PDD, profiles, cone factors, insert factors, and virtual source positions.

The commissioning measurements should be made by a qualified medical physicist. The procedures described in this report should assist in either measuring a complete set of beam data, or in verifying a subset of data before initial use or for periodic quality assurance measurements. TPS related commissioning data, as described by TG-53 (Ref. 2), should also be considered.

I.B.2. Issues with beam commissioning measurements

Even though most of the beam data measurements seem relatively simple, results could vary significantly depending upon the detector system and the phantom used. With availability of a large selection of radiation detectors covering all sizes (regular, mini- to microdetector), type (ionization chamber, semiconductor, etc.), and shapes (thimble, spherical, plane parallel), the choice of a proper detector can be overwhelming. In some situations, an improper choice of a detector may lower the quality of the collected beam data. An example of this is found in Fig. 1 that shows a wide variation in PDD of a 6 MV beam obtained with a variety of detectors for small, reference (10×10 cm^2) and large fields. The variations seem unforgiving for small and large fields.

Manufacturers often provide guidelines and tolerance limits for acceptance testing of a machine through their acceptance testing procedure. However, machine commissioning is the responsibility of the institution's qualified medical physicist. Previous task groups[14,15] provided guidelines for acceptance testing but provided no information for commissioning beam data. The recent publication[16] on acceptance testing and commissioning of linear accelerator provided details of acceptance testing of various components but did not address the commissioning aspect. There is a misconception between acceptance testing and commissioning. The acceptance testing implies the verification process of the machine based on manufacture's guidelines for a very small subset of beam data whereas commissioning is a process where a full set of data is acquired that will be used for patient treatment. There is very little information available in the literature for machine commissioning in providing dosimetry data for clinical use in radiation oncology.

I.B.3. About this task group

This task group was formed to review the physics of commissioning linear accelerators and to provide guidelines and recommendations on proper selection of detector, phantom, and methods to reduce measurement errors below $\pm 1\%$ in beam data acquisition. This task group does not provide the gold standard data for a machine nor does it deal with data collection for a specific TPS. However, the task group has attempted to cover the breadth of data collection as completely as possible. The charge of this task group was aimed directly at detectors and techniques for "beam data commissioning," characterizing and documenting beam-specific behavior which is typically then used for commissioning dose calculation algorithm behavior. Although inhomogeneity correction is an important aspect to characterize, especially for contemporary algorithms (Monte Carlo and convolution/superposition) those kinds of commissioning checks are significantly more difficult to perform and are dependent on the treatment planning systems. Therefore, it seems quite reasonable for the TG report to note that the inhomogeneity measurements are an important part of commissioning, but that they are beyond the scope of the current task group report and need to be addressed by a future task group. It is also

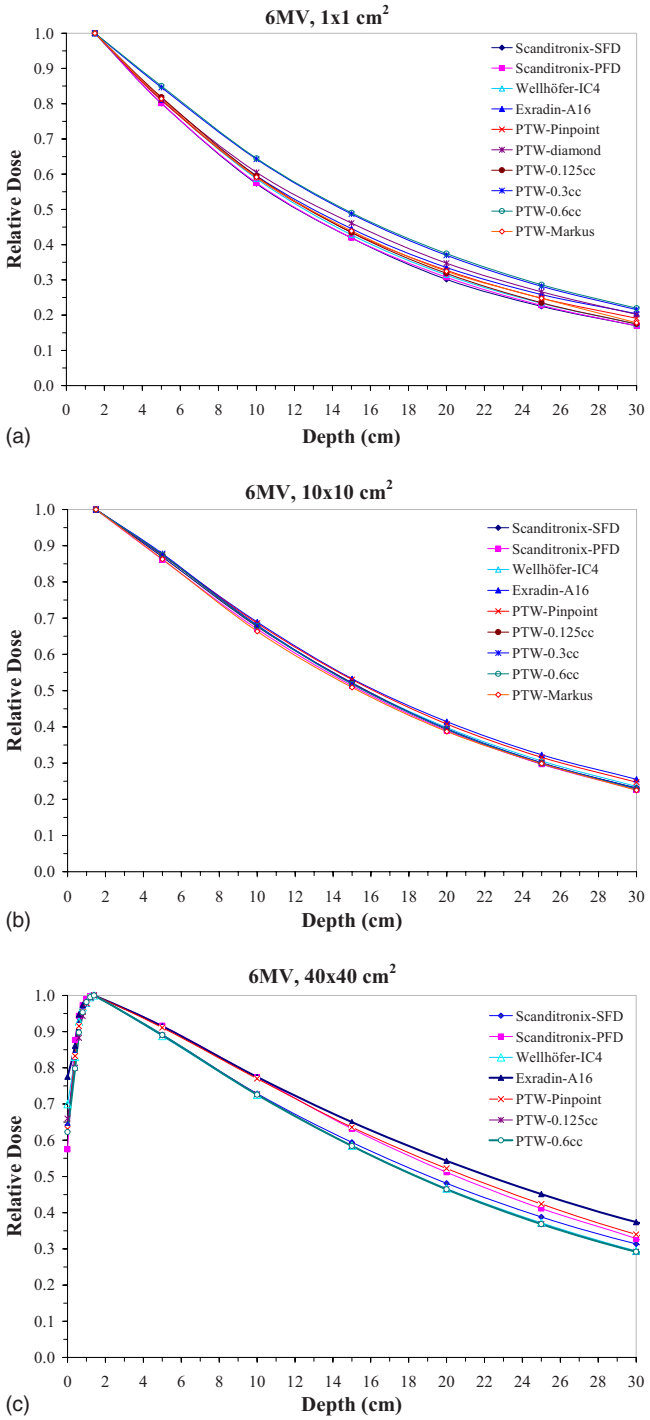

FIG. 1. Depth dose data for a 6 MV beam for (a) 1×1 cm^2, (b) 10×10 cm^2, and (c) 40×40 cm^2 fields using different detectors.

recognized that there may be an overlap of materials with other task groups such as stereotactic radiosurgery (SRS),[17] intensity modulated radiation therapy (IMRT),[18,19] head scatter (TG-74),[20] film dosimetry (TG-69),[21] electron beam (TG-70),[22] and other reports. Where appropriate, this task group refers directly to those reports. TG-106 provides recommendations and guidelines for machine commissioning, such as comprehensive data on detectors, phantoms, measuring devices (electrometer), limitations, and corrections for commercially available systems. However, it is beyond the scope of this task group to provide guidelines for any special procedures such as SRS,[17] Gamma Knife, CyberKnife, total skin electron therapy,[23] and total body irradiation.[24] This task group is limited only to the beam data commissioning for linear accelerators, i.e., photon and electron beams.

I.B.4. Commissioning effort

The amount of commissioning data requirements depend on the user's clinical need, including the TPS, monitor unit programs, in-house data tables, etc. Tables I(a) and (b) show a sample list of beam commissioning measurements for photon and electron beams. The large amount of commissioning data from 1×1 cm^2–40×40 cm^2 fields and depths ranging from 0 to 40 cm is further compounded by the number of radiation beams available from modern accelerators; 1–3 photon energies and 0–8 electrons energies, making the commissioning of a modern accelerator an enormous task. It is important that the time allowed for commissioning is determined based on both the amount of data to acquire and the availability of the physics staff. An estimate of the data acquisition time should be made prior to machine acceptance. For example, the time required for scanning six data sets (one PDD and five depth profiles) for 15 field sizes for each of five beam modifiers (one open and four physical wedges) for a dual energy accelerator could be estimated as in Eq. (1) below

$$\begin{aligned}\text{Time} \approx\ & [(\text{PDD} + 5\ \text{profiles})/\text{beam energy}] \\ & \times(\text{open} + 4\ \text{wedges}) \times (60\ \text{points/scan}) \\ & \times[1\ \text{s/pts} + 1\ \text{s(movement and delay)}] \\ & \times 15\ \text{fields} \times 2\ \text{energies} \approx 9\times10^5\ \text{s} \approx 30\ \text{h}.\end{aligned} \tag{1}$$

To account for equipment setup, change in machine parameters, machine faults, etc., typical time for photon beam scanning is 1.5 weeks. An additional week is needed for point data collection, 1–2 weeks for electrons, and a week for verification. Typically, 1–2 weeks are needed in analysis and report writing. The typical time allotted for the commissioning process is 4–6 weeks. However, additional time estimates should be made for integrating nonscanned data measurements, baseline QA readings, benchmarking, a validation of TPS data, etc., that required to be performed. The time allowed for commissioning may place pressure on the physics staff to complete the task promptly, especially in clinics with minimum physics support. Attempting to perform the commissioning quickly with minimal qualified medical physics staff may affect the quality of the data collected.

If there are multiple machines of the identical type and matched beam characteristics, there could be a fairly good agreement in the beam data, as described by Marshall[25], for low energy beam. However, quantitative evaluations of beam matching for modern machines using one-dimensional gamma analysis[26] showed that 30% of the beam profiles do not match accurately. Reduction in time is possible by elimi-

TABLE I. (a) Typical commissioning measurements for photon beam data for each energy and wedge. (b) Typical commissioning measurements for electron beam data for each energy.

(a)	Description		Square field size (cm)															
			1	2	3	4	5	6	8	10	12	14	16	20	25	30	40	>40
		Application	IMRT data						Traditional radiation oncology fields									Magna field
	Scan data	PDD/TMR	×	×	×	×	×	×	×	×	×	×	×	×	×	×	×	×
		Profiles @ 5–7 depths Diagonal or star profiles	×	×	×	×	×	×	×	×	×	×	×	×	×	×	×	×
	Nonscan data	S_c	×	×	×	×	×	×	×	×	×	×	×	×	×	×	×	×
		S_{cp}	×	×	×	×	×	×	×	×	×	×	×	×	×	×	×	×
		WF/TF				×	×	×	×	×	×	×	×	×	×	×		
		Surface dose	×	×	×	×	×	×	×	×	×	×	×	×	×	×	×	×

(b)	Description		Cone size (cm × cm)				
			5×5	10×10	15×15	20×20	25×25
	Scan data	PDD	×	×	×	×	×
		Profiles @ 5–7 depths	×	×	×	×	×
	Nonscan data	Cone factor	×	×	×	×	×
		Cutout factor	×	×	×	×	×
		Virtual source	×	×	×	×	×
		Surface dose	×	×	×	×	×

nating full length of the commissioning for identical machines only when a proper analysis of a sample data set is conducted and agreement is within institutional tolerances, typically $\leqslant \pm 1\%$. Further time savings could be achieved by reducing the time per point acquisition, increasing the scanning speed, and reducing the time delay between successive measurements. However, reducing these scanning parameters may compromise the quality of beam data. Before embarking in such time saving measures, it is recommended that trial scans (e.g., large field beam profile scans) be performed to insure that errors are not being introduced into beam data collection.

II. PHANTOM MATERIALS, METHODS, AND DETECTORS

II.A. Phantom material

There are two types of data that are acquired during commissioning, as shown in Table I: (i) scanned data and (ii) nonscanned data or point dose data. Point dose data can be measured in a solid phantom (discussed later) or in a water phantom. Scanned beam data collection is carried out with a scanning water phantom; typically, a plastic tank filled with water to a level deep enough to allow central axis PDD and profile measurements to a depth of 40 cm. There are several variations of two-dimensional and three-dimensional (3D) water phantoms. Water tanks that are not large enough to permit at least a 40×40 cm^2 field and a scanning depth of 40 cm should not be used since full scatter condition will be compromised with possible errors. Scanning systems for photon beams should allow scanning in both cross- and in-planes (x and y directions). Scanning in both dimensions provides convenience and avoids alignment problems associated with tank rotation. For some TPS, data are required only for fields defined by the primary jaws, and the MLC is modeled in the TPS. However, measurements for MLC shaped fields are still needed for verification of the models.

If water is stored in a reservoir and pumped into the scanning tank, care must be taken to use distilled water with the addition of biocidal chemicals to prevent growth of algae that interferes with the driving mechanism. If a storage tank is not available, it is recommended that the temperature of the tap water be monitored when filling the tank and the temperature of the water in the tank should be at room temperature before starting measurements. Thermal response for some chambers are not fully accounted for, and hence, it is advisable to maintain the temperature very close to the room temperature.[27] Thus, it may be necessary to let the water sit for a period of time to equilibrate with the room temperature.

Since beam scanning usually takes more than several days, it is not uncommon to have algae buildup in the water after a few days of scanning. This is indicated by a change in

TABLE II. Physical characteristics of commerically avialable water equivalent materilas. NA: Nuclear Associates, NY; Radiation Product Design, Albertsville, MN; RMI. Radiation Measurements, Inc., Middleton, WI; CIRS: Computerized Imaging Reference Systems, Inc. Norfolk, VA.

Material, manufacturer	Color	Density (kg/m^3)	$(\mu_{en}/\rho)^{water}_{med}$ 6 MV	10 MV	15 MV	18 MV
Polystyrene, NA, RPD	Opaque	1050	1.035	1.037	1.049	1.059
Acrylic/PMMA, RPD	Clear	1185	1.031	1.033	1.040	1.044
Solid water, RMI	Maroon	1030	1.032	1.039	1.049	1.052
Plastic water, CIRS	Lavender	1012	1.032	1.031	1.030	1.030
White water-RW-3, NA	White	1045	1.035	1.036	1.049	1.056

appearance of the water in the tank, from clear to a somewhat murky looking. An effective way to remove the algae from the water is to add a very small amount of laundry detergent or chlorine. This should be done before scanning or as soon as the water appears to be murky. An additional advantage of detergent in water is to reduce the surface tension to help visualize the exact position of the detector during setup. Most scanning system manufactures also provide chemicals to add to the water to safeguard the hardware.

Additionally, evaporation of the tank water is common over the course of the scanning. Depending on the size of the tank, evaporation can sometimes lead to a measurable change in detector depth. It is recommended that the water surface be verified periodically, especially during long periods of scanning. Upon completion of beam scanning, the tank should be completely drained and dried. In some cases, a small amount of oil should be kept on the scanning hardware. It is advisable especially not to leave tap water in the scanning tank for a long period of time after scanning as mineral deposits and algae growth can damage the scanning mechanisms and may void the warranty of the scanning system.

II.B. Dimension of phantom

The size of the water tank should be large enough to allow scanning of beam profiles up to the largest field size required (e.g., for photon beams, 40×40 cm^2 with sufficient lateral buildup (5 cm) and overscan distance. Some planning systems require larger lateral scans and diagonal profiles for the largest field size and at a depth of 40 cm for modeling. To determine the appropriate size of the scanning tank, the overscan and the beam divergence at 40 cm depth should be considered. A factor of 1.6 times the maximum field size should provide a safe limit. Simple calculation shows that a tank size of 75×75 cm^2 is an optimum recommended size. If the scanning software does not have the ability to perform diagonal scans, the table pedestal should be rotated to acquire the desired data. In general, collimator rotation does not provide the flattening filter information that diagonal profiles are intended to provide, and hence, such data should not be taken with collimator rotation.

For diagonal profiles, the size of the tank could be much larger than 75×75 cm^2 with the same overscan distance. In practical terms, however, very few commercial scanning systems are capable of scanning the full diagonal plus 5 cm overscan at depths of >30 cm for a 40×40 cm^2 field at 100 cm SSD. Some compromise could be made by taking only half scans. Consequently, half scans will have to be collected for maximum field sizes that require an offset of the tank relative to the central axis. Before setting up for half scans, it is important to verify that the open beam show minimal asymmetry ($<0.5\%$) so that a half beam profile may be mirrored to represent the entire beam. It is also advisable that the half field scan be extended at least 5 cm past the central axis on the short side so that there is sufficient lateral buildup for the central axis at deeper depths. Half-field scans require more setup time. Some data maneuvering may also be required to generate a complete set of scans, depending on planning system requirements. Whatever time-saving procedure is used to cover the area of interest, make sure that it is compatible with the system using the data as input.

II.C. Solid phantom

Point dose and nonscanned (integrated) measurements, such as output factors, surface dose, leakage/transmission, wedge and tray factors, etc., can be measured in a water phantom, and can often be performed with the scanning system. However, solid phantoms that mimic water may be used for convenience. Other plastic material such as acrylic or polystyrene should be used with caution, as data collected with these materials may result in values that may require additional corrections due to differences in electron density, stopping power (S) and energy absorption coefficient (μ_{en}/ρ) as noted in Table II and various references.[28,29] Tello *et al.*[29] showed that radiologically solid phantoms differ from water in electron and photon beams depending upon beam energy. It was pointed out that solid phantoms do not truly represent the radiological properties of water.

A solid phantom should have an appropriate cavity drilled for tight fit of the detector which should be verified with a radiograph taken with low kVp with the detector inserted in the phantom. Different slabs of phantom should be used for different designs of the detector to ensure that a tight fit is maintained for each detector. When detectors are placed in a solid phantom, enough time should be given to thermally equilibrate with the temperature in the cavity.[30] The quality of the phantom material should be checked with a computed

tomography (CT) scan for any artifacts and inhomogeneity in electron density via CT number. Note that these CT numbers may differ from water if the solid materials are designed to be water equivalent at megavoltage energies only.

II.D. Buildup cap

For the in-air collimator or head scatter factor (S_c) measurement, a buildup cap, and/or a miniphantom is traditionally used. Commercially available buildup caps (Radiation Products Design, Albertville, MN)[230] are inadequate to remove contaminant electrons at the energies for which they are rated. TG-74 (Ref. 20) recommends a miniphantom to provide electronic equilibrium and elimination of contaminant electrons provided that the field covers the miniphantom completely. For small field sizes ($\leqslant 4\times 4$ cm^2), extended distance (e.g., source-chamber distance 300 cm) can be employed if one has to use the same water-equivalent miniphantom. TG-74 recommends that a preferable solution is to use a high-Z miniphantom and all S_c measurements be made at the same distance. Thus, a metallic miniphantom can be used at the isocenter because of its much smaller size[31] provided appropriate correction factors are applied as recommended by TG74.[20] Typical longitudinal thickness of a miniphantom is 10 g/cm^2, although other thicknesses can be used as long as a correction factor is applied.[32] A detailed description and recommendation can be found in TG-74.[20] It is important to choose a buildup cap of sufficient thickness in S_c measurements, otherwise erroneous S_c data will be obtained. Further discussion on the fundamentals of the output factors can be found in Sec. IV C.

II.E. Detectors

II.E.1. Availability of detectors

Various manufacturers offer a wide range of radiation detectors including ion chambers, diodes, diamond detector, and other types. These detectors can be categorized in terms of their size as standard, mini- and microdetectors. Even though there is no clear definition, ionization chambers could be divided by their active volume as indicated below:

- Standard chamber ($\approx 10^{-1}$ cm^3)—The active volume for a standard Farmer-type ionization chamber is on average 0.6 cm^3.
- Minichamber ($\approx 10^{-2}$ cm^3)—The active volume for a mini-ionization chamber is on average 0.05 cm^3.
- Microchamber ($\approx 10^{-3}$ cm^3)—The active volume for a microionization chamber is on average 0.007 cm^3 and ideally suited for small field dosimetry such as radiosurgery, gamma knife, CyberKnife, and IMRT.

II.E.2. Detector types

II.E.2.a. Ion chambers. Ionization chambers have been used since the discovery of radiation and are still widely used due to their small variation in response to energy, dose, dose rate, and reproducibility. Since chambers can be calibrated against a national standard, they can provide a direct measure of the dose. Ion chambers are relatively inexpensive, readily available, and are manufactured in various shapes (cylindrical, spherical, and parallel plate) and sizes (standard, mini, and micro). Humphries and Purdy[33] provided a list of chambers and their characteristics for beam data scanning. However, most vendors are now marketing different ion chambers for a variety of applications in radiation dosimetry. An assortment of radiation detectors for specific tasks can be acquired from various manufacturers (i.e., PTW, BEST, IBA, Standard Imaging, etc.) based on the latest research and need.

II.E.2.b. Diodes. Semiconductor diode detectors are used widely for beam data commissioning for both photon and electron beams. Characteristics of diodes include quick response time (microseconds compared to milliseconds of an ion chamber), excellent spatial resolution, absence of external bias, and high sensitivity. In addition, diodes provide energy independence of mass collision stopping power ratios (between silicon and water for clinically usable electron beams with energy between 4 and 20 MeV).[34–36] Thus, diodes are particularly attractive for radiation dosimetry in an electron beam. It is important that specific types of diodes should be used for specific radiation and hence electron diodes should only be used in electron beam and photon diodes should be only used in photon beam. The response of the diode detectors depends on temperature, dose rate (SSD or wedge), energy,[34,36–38] and some may have angular dependence as well. In order to achieve the required accuracy recommended by TG-62 (Ref. 39), either these effects should be corrected or a diode with minimum dose rate and energy dependence should be used. There are conflicting publications on the use of diode detectors for beam data acquisition,[40–43] hence, before using a diode detector, one should compare it with ion chamber measurements to confirm its correct operation and accuracy in data.

II.E.2.c. Detector arrays. A detector array system can be used for simultaneous data acquisition over the entire open beam and offers the most suitable method for soft wedge (dynamic wedge or virtual wedge) profile measurements. The array system may be an ion chamber array (air or liquid-filled) or a diode array, depending on the manufacturer. Since an array consists of several detectors arranged in a linear fashion, the array must be calibrated in a field size recommended by the manufacturer to set the amplifier gain of each detector before it can be used for the scanning. Often these detectors are calibrated from the factory with proper gain; however, it should be checked for accuracy before use. It has been noted that there is no difference between diode and ion chamber array for dynamic wedge data measurement, and hence, either of these systems could be used.[44,45]

II.E.2.d. Diamond detector. Diamond detectors are a solid-state radiation detector with a high electron and positive hole mobility making them attractive semiconductor detector for ionizing radiation. The theory of diamond detectors is very similar to that of diode detectors. When ionizing radiation is absorbed, it induces a temporary change in the electrical conductivity of the material.[46–50] The response of a diamond detector is directly proportional to the absorbed dose rate. Diamond detectors do not exhibit any directional

dependence and they are tissue equivalent. The sensitive volume is small (1.0–6.0 mm^3), which makes it ideal for small field dosimetry and for profile measurements. Diamond detectors do exhibit a small dependence on dose rate. They can be used in water with any scanning system for data commissioning. The diamond detectors are difficult to manufacture and hence are more expensive than other solid state detectors.

II.E.2.e. Thermoluminescent dosimetry. Thermoluminescent dosimetry[51] (TLD) has been used for point dose measurements and *in vivo* dosimetry. The TLD material comes in several different forms, such as rods, chips, and powder. Rods and chips are reusable once they have been properly annealed. TLD exhibits strong energy dependence, fading, and nonlinear dose response. However, these effects in megavoltage beams are relatively small.[52,53] The accuracy is limited to the irradiation and measuring techniques. Typically an accuracy of less than ±5% (Ref. 54) can be achieved. For the Radiological Physics Center and calibration laboratories, accuracy on the order of ±1% is achievable. TLD is usually not suitable for data commissioning except for verification and cross reference of point dose in small fields and IMRT.

II.E.2.f. Film. Film is used for dose measurement based on optical density variation that is generally dependent on field size, depth, beam energy, processor condition, and other factors as described in TG-69.[21] There are two types of films; silver halide and Gafchromic. TG-69 and TG-55 (Ref. 55) provide overviews of silver halides films, and Gafchromic films, respectively. Silver halide films exhibit strong energy dependence for photon beams but their response is relatively independent in megavoltage electron beams. Due to this reason film could be used for electron beam.[22,56] Beam data acquired with films may not be as accurate as data acquired with ion chambers. However, film does provide an opportunity for acquiring planar dose maps in small fields[57,58] and for soft wedges.[59] When film is used for small field dosimetry, blurring due to film scanner should be considered as observed by Yin.[60]

II.E.2.g. Metal–oxide–silicon–semiconductor field effect transistor (MOSFET). MOSFET dosimeters have been investigated for their use in clinical dosimetry[61] and IMRT verification.[62] Due to their small size, MOSFETs are ideal for small field dosimetry, brachytherapy, and *in vivo* dosimetry. MOSFET dosimeters are similar to conventional dosimeters in reproducibility, linearity, energy, and angular responses.[61] The MOSFET detectors have a short life span (total dose) and are not suitable for beam commissioning but can be used for specialized point dose measurements.

II.E.2.h. Bang gels. Bang gel detectors[63] are tissue equivalent and provide a 3D dose map with high spatial resolution. They are energy independent over a wide range of energies, making them ideal for measuring three-dimensional dose distributions. In order to generate an image of the dose distributions, the gel needs to be imaged by using magnetic resonance imaging, x-ray computed tomography, or optical computer tomography. Each of these imaging techniques is susceptible to imaging artifacts. In general, the use of gels is an extensive process and has limited usefulness in beam data commissioning except for SRS and IMRT.

II.E.3. Selection of detectors

Ion chambers, diodes, and diamonds are well suited for commissioning beam data in a scanning water phantom. Ion chambers are by far the most commonly used due to their availability, the relatively low cost, accuracy, and ease of application. The selection of detectors should be carefully examined with the type of application, field size, resolution, and time needed to complete the data collection. For example, most scanning systems utilize ion chambers with an inner diameter of 4–6 mm, which is adequate for field sizes $\geqslant 4\times 4$ cm^2. However, these chambers are not appropriate for the small field data required for IMRT and cannot describe correctly the penumbra region due to blurring. Rather small volume ion chambers or diodes are often used for small fields $\leqslant 4\times 4$ cm^2.[64–68] Small volume chambers and diodes tend to have different characteristics for large fields compared to small field and should not be used for all field sizes unless it can be documented that accurate data can be acquired for all field sizes. Small field profiles should be measured with microchambers such as stereotactic field diodes or pinpoint ion chambers. Since signal in these detectors are relatively small, scanning (sampling) time should be increased to improve the signal-to-noise ratio as discussed in Sec. III A 3 g.

II.E.4. Detector response and corrections

The finite size of the detector provides an average response over the sensitive volume that smears the profiles. When small volume detectors are not available, a deconvolution method[69–76] could be used. It has been proven definitively that the broadening of the measured penumbra due to the detector size could be explained by the detector convolution kernel.[70–76] It is possible to extrapolate the true penumbra using the detector convolution kernel. Deconvolution algorithms are susceptible to noise and require tuning to eliminate the noise effect.[72] This problem could be solved if both the penumbra and detector convolution kernel are expressed as analytical functions. Several studies have provided analytical expressions for the penumbra[77,78] and the detector convolution kernel. To avoid such a lengthy process, user should choose a microchamber for small field measurement. The deconvolution method is complex and time consuming to be effective for a large number of profiles and should be reserved as a last choice for only a limited data set unless a commercial software is available.

III. SCANNING SYSTEM SETUP

Setting up the water phantom system properly can help improve the workflow, and more importantly, reduce the likelihood of collecting suboptimal data, which may result in a considerable amount of processing and sometimes may even require rescanning. Before setting up the water phantom and planning for data collection, check the existing

cable run. If existing cable runs cannot be used, it is necessary to run cables under or over the door. It is also beneficial to set up the scanning computer alongside the accelerator controls to reduce the unnecessary movement across the control area. This can trim considerable time from the total data collection time.

III.A. Verification and validation of scanner

Modern water scanning systems are extremely accurate and precise. However, some basic quality assurance as suggested by Mellenberg *et al.*[79] and Humphries and Purdy[33] should be adopted. A periodic quality assurance or at least before the use of the water tank may be warranted to check the free movement of each arm, and the x, y, z, and diagonal motion. Manufacturers of scanning systems offer annual preventive maintenance services that should be performed. Accuracy and linearity should be checked over the long range of the scanning system. Physical condition of the tank, such as leaks, cracks, and mechanical stability, as well as the quality of connecting cables for leakage and reproducibility should also be checked before the use of scanning system for commissioning beam data.[33]

When using a scanning system where all components are manufactured by the same vendor, it can generally be assumed that these components are matched to provide good data; however, the user should still verify that there are no defects or communication errors in any of the components. Furthermore, it is possible to add components, particularly detectors, from the same vendor and those components may not be compatible with the original scanning system. In house controllers to link scanner with accelerators to provide automated field change and batch job as described by Schmid and Morris[80] should be tested for flawless operation. Such futuristic interface devices are not yet available from commercial vendors.

There has been an increase in detector specialization. This may require the user to connect new accessories (detectors, cables, connector, adaptors) to an existing scanning system. The resulting scanning system may be a collection of components from different manufacturers and it is incumbent upon the user to verify the integrity of the hybrid system. Detector attachments typically require a proper attachment kit for a specific scanning system.

III.A.1. Scanning (field) and reference detectors

In general, two detectors are needed for scanning; a field or scanning detector that moves in the tank as programmed and a reference detector, which is stationary in the field. The use of a reference detector is strongly recommended for all scanning systems. This removes the instantaneous fluctuations or drifts in the incident beam output. Both the scanning detector and the reference detector must be securely mounted with custom or vendor specific holders in order to produce accurate and reproducible scans. Metallic adapters and holders should be avoided for securing the detector in the scanning system, as scatter radiation could affect the data accuracy. When using a detector, which was not originally supplied with the scanner, an appropriate adapter should be used from the manufacturer of the new detector. Do not attempt to tape or shim the detector into position since submersion into water may loosen such mounts and produce inconsistent data increasing the time for commissioning.

The reference detector may be positioned anywhere in the beam where it does not shadow the field detector for the entire area of programmed positions. For very small fields, where the reference detector may shadow the field detector, a time integration method could be used instead of the reference chamber. The field and reference detectors should be chosen based on the application of the beam data, as discussed earlier in this document. These two detectors do not have to be of the same type. However, when connecting these detectors to the scanner, the following parameters should be considered carefully.

III.A.1.a. Detector mounts. Generally, the detectors supplied with scanning systems have nearly identical dimension in active length and inner diameter. However, if this is not the case, consideration should be given to chamber dimension when determining scan directions. Apart from the dimension, the movement of the detector should be considered. With respect to the central axis of the beam, long axis of the detector could be mounted in three possible ways: (i) perpendicular but in gun-target direction, (ii) perpendicular but in cross-plane, and (iii) parallel to the beam. Detector orientation plays an important role in profiles and penumbra measurements, which will be discussed in Sec. IV A 4 a. Detector should be mounted such that the scanning arm has minimum volume in the scan direction. When parallel orientation is used, care should be taken for leakage and cameral effect as discussed in Sec. III D 4.

III.A.1.b. High voltage (bias). Most ion chambers are operated in the voltage range of 300–400 V. On the other hand, diodes must have zero bias. The diamond detector typically uses 100 V. It is recommended that before connecting the detector to the electrometer, the user should be familiar with the type and voltage requirement of the detector. It is a good practice to check the bias requirement while changing detectors in between data collection and before turning the electrometer to the ON position. Incorrect application of detector bias may damage the detector. Figure 2 shows PDD data collected with a chamber with excessive leakage (bad chamber) and a correctly functioning chamber (good chamber) with an incorrect and correct gain setting. An appearance of abnormal pattern or spikes observed in the scan data could be an indicator of improper detector bias and or gain. In such situation the scanning should be interrupted immediately and the detector bias should be checked properly.

III.A.1.c. Polarity. The polarity of an ion chamber signal is determined by the high voltage (HV) bias polarity and will not be an issue if the HV bias is controlled by the electrometer. However, diode signal polarity is determined by its internal construction. The diode manufacturer may offer both positive and negative polarity for the same model detector. Therefore, the user must ascertain when ordering the detector that the electrometer can accommodate the polarity. In general, most detectors can be operated with either polarity,

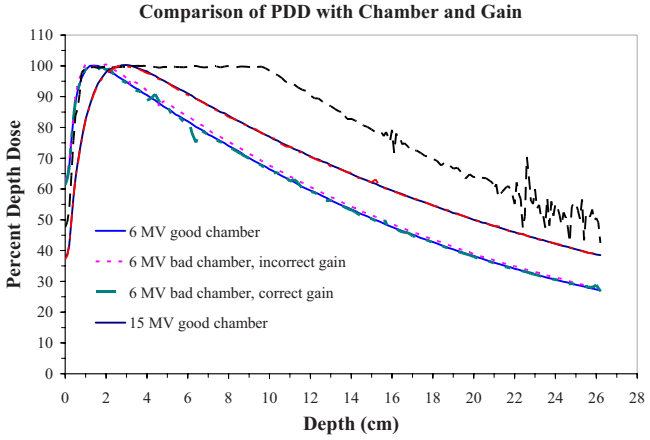

FIG. 2. Comparison of depth doses with good and bad chambers with correct and incorrect bias.

however, the user should make sure that data collected in the positive (+) polarity is in agreement with the negative (−) polarity. Figure 3 shows the ratio of PDD taken with positive and negative (±) polarity for various detectors. The line at 1.0 corresponds to no polarity effect and either polarity can be used. Large deviations could be observed for some detectors in Fig. 3. Kim *et al.*[81] provided the magnitude of polarity effect in thimble ion chamber at low dose rate that also needs to be clearly evaluated. In general, some differences with ± polarity are expected. However, the difference should be less than 0.5%. It is recommended that data collection be performed at a consistent single polarity that is reproducible in repeated measurements. Differences, as noted in Fig. 3, can be avoided by selecting one polarity for the entire scanning and choosing an appropriate detector that has minimum polarity effect.

III.A.1.d. Recombination. Ion recombination is generally not a problem in most ion chambers that are designed specifically for scanning at relatively high (≤300 V) voltages. Check the manufacturers' recommended bias settings for the scanning chamber. Some small volume chambers may have a lower recommended voltage bias than the standard 300 V. If possible, set the bias at half voltage and check the recombination effect[82] at the dose rates used during scanning to verify that no recombination correction is needed.

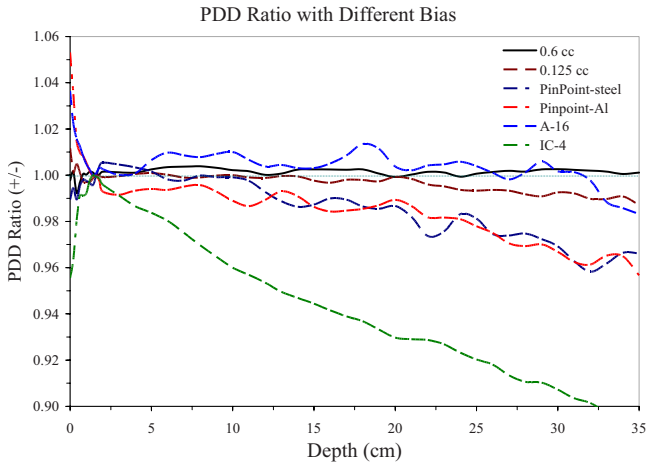

FIG. 3. Ratio of depth doses with positive and negative (±) polarity on various chambers.

III.A.1.e. Sensitivity. The sensitivity of the detector must be sufficient to provide a reasonable signal-to-noise ratio in the electrometer but not as high as to cause signal saturation. The measurement range of the electrometer should be checked before scanning. The sensitivity of the detector should be available from the detector manufacturer. The sensitivity of the field and reference detectors should also be balanced. Some scanning software packages adjust the gain automatically in both the field and reference electrometers to equalize the signal. It is a good practice to check the gain of both detectors when field size is changed. Of course, the gains may need adjustment when scanning is switched from open to wedged fields.

III.A.1.f. Energy response. In general, ion chambers have an almost constant energy response for megavoltage photon beams and can be used without corrections. Diode detectors, on the other hand, may have an energy response in photon beam that may affect the scanned data. The diode energy response can be detected by comparing its PDD for 6 MV in a large (40×40 cm^2) field with the corresponding ion chamber measurement. If the diode curve does not drop off as rapidly as the ion chamber PDD, then this is an indication of energy response. Generally, diodes should not be used for PDD measurements in large x-ray fields, unless specific compensation or corrections with validated test results indicate otherwise.

III.A.2. Cables, connectors, and adapters

The integrity of scan data requires a high quality cable and electrometer; otherwise, the detector signal can be influenced by many subtle factors that will lead to incorrect beam data. Some of these factors are related to the fidelity of the cable, quality of connections, and adapters. Users should be aware of various types of connectors, which are discussed below.

III.A.2.a. BNC and TNC connectors. The BNC (Bayonet Neill-Concelman) is named after its inventor and has a twist-on attachment, like a bayonet. It is made for both coaxial and triaxial cables. TNC (Threaded Neill-Concelman) is a threaded version of the BNC connector. Both of these connectors are used in dosimetry and some familiarization is important. Figure 4 shows examples of these connectors. The BNC and TNC connectors look alike from outside. Connectors come in various types (TNC, BNC, etc.), sexes (male, female), and conductors (triaxial, coaxial). The examples in parenthesis are most common among radiation detectors and electrometers used in water tanks. One vendor has a modification of a "triax" connector, which appears as a coaxial and an electrical pin inside the connector housing. Details of these connectors can also be acquired from various vendors such as CNMC, Standard Imaging, PTW, and Wellhöfer. It is always helpful to mark these connectors when they arrive from vendors for future use.

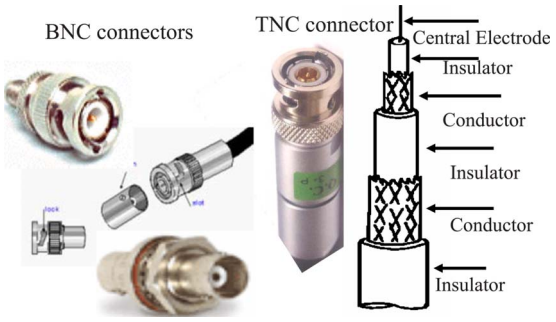

FIG. 4. BNC, TNC, and components of the triaxial cable.

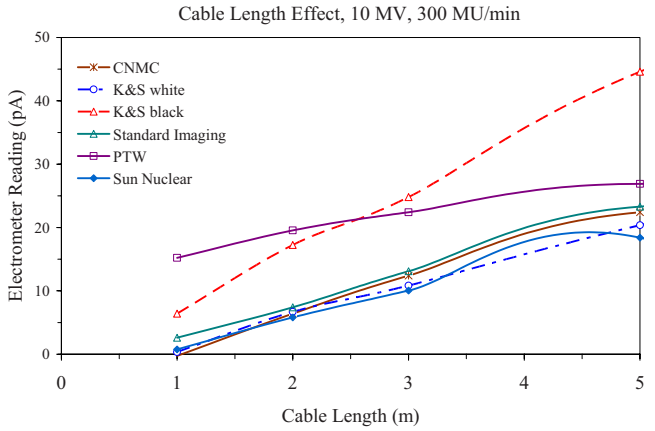

FIG. 5. Effect of cable length in radiation beam. The cables are of different types from various manufacturers.

- Male: Center conductor is a pin
- Female: Center conductor is a socket hole
- Triax: Three-conductor cable or connector, all concentric
- Coax: Two-conductor cable or connector, all concentric
- Adapter: A connector union or short cable with two ends that connect to different connector types.

III.A.2.b. Common connection errors. Most cables used in radiation dosimetry and with the scanning system have triaxial adapter ends with male and female connections. Ion chambers are directly connected to the triaxial cable end. Some manufacturers market unusual looking triaxial ends (nonstandard) that may not fit standard ion chambers. If such a situation is noticed, special adapters from manufacturer should be acquired. PTW is one such vendor that has different triaxial adapter ends. With a diode, there are two electrodes (anode and cathode) and these require a coaxial cable. Ion chamber connectors have three electrodes (collector, guard, HV bias) that require a triaxial cable. It is possible, with proper adapters, to use a triaxial cable with a diode detector, but the reverse is not applicable, i.e., a coaxial cable cannot be used with an ion chamber. Furthermore, since there is high voltage in the ion chamber cables, care must be taken that there is no shock hazard to personnel or to sensitive electronic equipment. It is imperative that every connection be made only with the equipment powered off.

Forcing a coax BNC connector into a triax BNC connector is the most common error when trying to connect a diode detector into an electrometer designed for ion chambers. Two serious problems can happen: (1) damage to the connector by forcing the coax and triax together, and (2) the electrometer's high voltage bias supply is shorted with improper connection that may damage the detector or electrometer. Do not force, twist, or turn the cable as that may short the bias when connecting. Even with inaccurate connection one may still see some signal. However, such signals are nonreproducible.

III.A.2.c. Leakage current. Every cable used in data collection has a certain amount of leakage current that depends on the quality, upkeep, and handling of the cable. Heavily twisted and badly bent cables may result in significant cable noise. Most commercially available cables have a leakage level in the range of 10^{-13}–10^{-14} A.[83–85] The leakage is significantly higher for poorly kept, twisted, and kinked cables. When data are collected in small fields or beyond the field edge, the leakage signal can overwhelm the measurement signal. Leakage noise current is typically dependent on the quality of the cable, length of the cable in the beam, and connectors. Some electrometers have leakage, zero, or null circuit options, to offset any leakage. If such option is available, it should be used to offset the leakage signal with beam off. The orientation of the detector mount also affects the amount of cable in the beam which may introduce a leakage signal.

Figure 5 shows the effect of cable length in the radiation beam for various types of cables from different manufacturers. The amount of cable in the beam could be a serious matter in electron beam which was discussed by Das *et al.*[86] Special precaution is needed when large amount of cable is kept in the radiation beam. Prior to scanning, one should inspect the cable length for kinks and nicks in the jacket, particularly the length near the detector where it will be submerged. A sharp kink and nick can cause discontinuity as well as damage the inner dielectric insulator and the noise reduction coating, which may cause electrical problems in the electrometer when submerged.

III.A.3. Electrometers

Electrometers used with a water scanning system have a high degree of fidelity with a wide dynamic range. They can measure charges in the range of 10^{-6}–10^{-14} C. Electrometers should be reset to null or zero before scanning. The user should verify that the response is linear before measuring any data in various gain range settings. A collected reading is a composite response of the detector and electrometer. The detector response is typically microseconds (μs), whereas electrometers are millisecond (ms), hence, electrometer response is much critical in scanning.

III.A.3.a. Measurement polarity. There are two types of input polarity to an electrometer: bipolar and unipolar. Bipolar electrometers can measure input signals of both positive and negative polarity. Unipolar input can only measure input signal with one polarity. See the discussions above on polarity and leakage.

III.A.3.b. Input offset current (leakage). In addition to the signal current, an offset (leakage) current contributes to the measurement signal. In most systems, this should be an insignificant contribution. However, it may become significant and cause offsets in the profile measurement especially with insensitive and small volume detectors as discussed above on leakage current.

III.A.3.c. Input offset voltage. Electrometers also have an input offset voltage between the inverting and noninverting inputs. The electrometer's basic operating principle maintains these two inputs at (or near) the same voltage. If this offset voltage is significant, for example greater than 1 mV, then different effects can occur. With an ion chamber, there will be an offset in the signal measurement, much like the effect of input offset current. If measuring with a scanning diode, this offset voltage is directly across the diode and will cause current to flow, just as if it were coming from the diode signal.

III.A.3.d. Continuity. Another issue with small dimension chambers is reasonably good ion collection with a low voltage bias. Even voltages as low as a few millivolts can provide reasonable (but not saturated) ion collection. These are the types of voltages present at the electrometer input offset between guard and electrode. If an HV bias is failing or if there is not good contact to the chamber HV electrode, one may still collect what appears to be a good signal. Apart from invasive testing, there is limited testing to assure good continuity. One method, if the electrometer and bias control permit, is to change the polarity, when collecting beam data, to see if the signal polarity changes as well. If so, then the change in signal polarity is likely due to the bias change because the stray contact and input voltage offsets will generally not change with the bias polarity switch.

Another problem with continuity could occur when the scanning chamber and cable are submerged in the water tank. If proper care is not taken in the connections, adapters, cables, etc., a "short" of the bias supply to the chamber could occur under the right conditions. Comparison of scans in the dry run and water run tests described below could show a difference. In addition, the polarity reversal test in the above paragraph would also show a problem.

III.A.3.e. Gain and autorange change. Electrometers may have different gains that allow the use of a variety of scanning detector sensitivities. The gain can be adjusted either manually or automatically. If it is a manual system, the gain should be checked for both field and reference chambers such that they produce nearly identical readings at a reference point.

III.A.3.f. Signal saturation. Use of a scanning detector that is not included with the original design of the scanning system may cause the electrometer to over-range. Some of the small volume ion chambers have sensitivities of 0.5 nC/Gy, whereas some diodes could have sensitivities of 50 nC/Gy or more. This is a difference of a factor of 100. Thus, measuring with a diode on an electrometer setup for small ion chambers may easily saturate the electrometer. Any abnormal scan should be analyzed in the context of signal saturation. Such a scenario often happens in wedge profiles where signal range varies significantly from toe to heel of the wedges.

III.A.3.g. Signal-to-noise ratio. The opposite of signal saturation is "not enough signal" above the noise level, i.e., low signal-to-noise ratio. The signal-to-noise ratio should be kept high by choosing proper detector, gain, and good quality of cables with minimum noise. If scanned data are not smooth, especially in the penumbra region for photon beam and bremsstrahlung tail for electron beam, one should look into the signal-to-noise ratio. A factor of at least 100 for a signal-to-noise ratio is a good criterion that should be maintained for scanning.

III.A.3.h. Response time. The response time of the electrometers determines how quickly the changing signal is tracked and measured. The signal from the scanning detector changes very quickly at the beam edge with high speed of scanning. If the response time is too long and the scan speed is fast, this will result in penumbra broadening. It is difficult to generalize and provide numerical values since scanning systems use different approaches and varied response time. Modern scanning systems have speed from 1 to 500 mm/s and typical response time of $\leqslant$10 ms. Hence, a high speed up to 100 mm/s may not be a problem.

III.B. Scanning water tank

III.B.1. Positioning and labeling

Positioning and labeling the tank appropriately is critical for ensuring the quality of data and/or detecting possible sources of error in scan data. The scanning tanks should never be placed on the machine treatment table as the water load could easily damage the table support mechanism. A typical large scanning tank with water weighs nearly 280 kg (616 lbs), which is well beyond the weight tolerance of the treatment tables. Most manufacturers provide a sturdy platform either over a water reservoir or stand-alone platform to support the tank. When setting up the tank, the orientation should be such that the chamber can scan with the least amount of moving parts. For example, on many 3D systems, the x scan dimension requires only the chamber to move along a scanning arm, whereas the y scan dimension requires the entire arm to move in the water. The x scan may give cleaner scans since less material is passing through the water, disturbing the water surface less. Position the tank based on the desired conventions of the scan and treatment planning nomenclature. Disturbing and transposing scanning tank labeling during commissioning is not recommended as it adds extra time and may confuse the machine parameters.

The tank origin (0,0,0) should be close to the machine isocenter. Otherwise, the offset could pose problems for large field measurements. A good practice is to align the tank with the lasers such that x axis is the cross-plane (left-right) and y axis is the in-plane (gun-target) direction. Differences about $\pm 1\%$ in x and y profiles could be expected and tolerated for most machines. For some linear accelerators like Siemens where beam steering is only available in the radial direction, x scans are smoother and less problematic. It is recom-

mended that manufacturer-supplied alignment devices should be used when available. Most scanners have a built-in labeling system, i.e., x, y, and z. It is advisable and expected that labeling is consistent with the TPS.

III.B.2. Scanner movement

Make sure the detector is level with the water surface in all four corners of the tank. If a vendor-provided alignment cross mark on the cap is available to check the horizontal level in all four corners of the tank, it should be used as it provides precise leveling of the tank. One can also use a mark on the detector or any other device to check the leveling.

III.B.2.a. Central axis scanner movement. The z-direction movement of the detector should be parallel and should follow the central axis of the machine at 0° gantry angle. One could verify the detector movement to follow central axis for depth dose by following methods:

- Check the vertical travel of the detector with a simple string plumb bob to make sure that the arm travel is exactly vertical.
- Close the jaws to a field size that gives about 1 mm flash on the sides of the detector and one jaw in the other direction gives about 1 mm flash on the end of the detector. Then by driving the detector from surface to depth, one can follow not only the location of the crosshair image on the probe, but also the relationship of the detector to the jaws. It is quite apparent if the probe "walks" when going from surface to depth.

If performing tests on the tank prior to each use, the above tests should be carried out with the tank full, as this influences leveling of the tank.

III.B.2.b. Zero depth. In setting the SSD, the distance should be verified by at least two methods, such as laser position on the sides of the tank and the ODI and/or a mechanical measuring stick. It is very convenient if the laser could be used as distance indicator. This would require the accuracy of the laser be verified. When the water surface is properly aligned with laser/mechanical pointer for 100 cm, the detector position should be set such that the center of the detector splits the water surface. This is easily done with a cylindrical chamber, when looking underneath at the reflection of the detector onto the surface of the water. The proper way to ensure that the center of the chamber is set precisely at the water surface is illustrated in Fig. 6 for the cylindrical chamber where the reflected image and the detector make a perfect circle. This position should be denoted as the zero position and should be set in the computer for scanning purpose. Water evaporation may cause a change in zero depth and should be checked at the beginning of the day and periodically (at least every 6 h) during the day. Some scanners have motors that displace water when they are immersed during scanning. The scanning software usually corrects for the change in depth based on the displacement. However, for a large tank such errors are relatively small. For these types of scanning system, operational instructions should be carefully followed and software compensation needs to be verified before use.

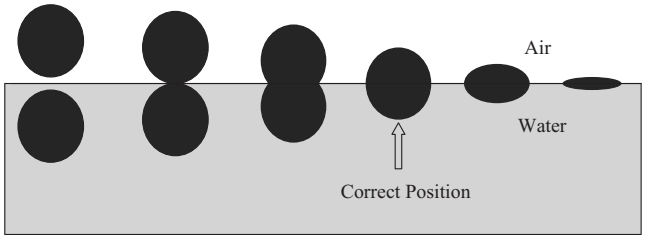

FIG. 6. Sequential appearance of chamber and its reflection in water viewed from tank side. The correct position is when both images form a perfect circle.

III.B.2.c. Chamber shift. With the tank and/or scanning arms leveled and the water surface at the correct SSD, the origin on the scanning system can be established. For some protocols, the center of the detector is not the point of measurements, and hence, the shift to an effective point of measurement is needed. The shift for photons is different from that of electrons and also different for different dosimetry protocols.[82,87,88] When a cylindrical ion chamber is used in a water phantom, the geometrical center can be accurately determined as shown in Fig. 6. The ion chamber shift can be made from this initial position. Many scanning systems will account for this offset in the software, and/or an option of performing a manual offset (turning software correction off) is provided. If the scanning software is used to correct for the offset, the depths associated with the measured data may be noninteger values. For most ion chambers, this offset is typically between 1.5 and 2 mm, and hence, the chamber should be lowered by the shift amount from the zero position. This will be then the correct position for scanning.

III.B.3. Orientation

Most scanning systems have an orientation method to define the relationship between the tank position and gantry axes. Typically the y axis is the gun-target and the x axis is the cross-plane direction. Make sure that this orientation is correct and that the motions are correct. Improper orientation and definition of orientation can compromise the data when input into a treatment planning system. For example, if the TPS reads scan data as if a 45° wedge scan was performed from the end of table to the gantry with the toe of the wedge facing the gantry, but in fact, the scan was really performed along the nonwedged direction in the transverse plane, this would seriously compromise data entry.

III.B.3.a. Axis alignment. For correct scanning, the tank must be positioned so that it is aligned with the radial (in-plane) y axis and transverse (cross-plane) x axis. This can be accomplished by aligning lasers to the alignment marks on the side of tank or aligning the probe holder to a field edge. This can also be checked by manually driving the probe along one of the axes while ensuring the center of the probe does not "walk" from the crosshair. If this is not done correctly, the field size of the profiles will not be correct and

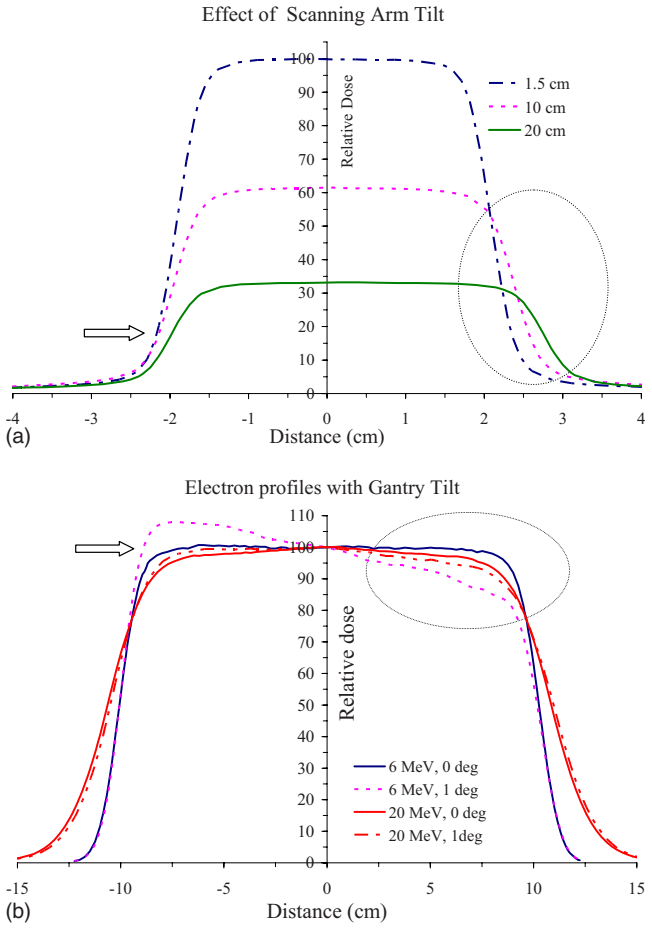

FIG. 7. (a) Beam profiles of a 6 MV beam at different depths with scanning arm tilt for a 4×4 cm^2 field, (b) electron beam profiles at depth of 80% depth dose for 20×20 cm^2 cone with gantry tilt. Arrows and circle are shown to represent the impact of arm and gantry tilt.

some profile data, such as wedge profiles, can be compromised. If photon and electron beam profiles do not look accurate, arm tilt and tank tilt may be responsible, as shown in Fig. 7, and corrective action should be taken.

III.B.3.b. Tank tilt. Leveling of scanning systems may involve leveling the entire tank or only the scanning arms using a precision level. For x rays, the effect of a tilt in the scanning arm will be a subtle change in symmetry, but a marked change in the centering of each individual scans, i.e., beam appears to become increasingly off center with increasing depth as shown in Fig. 7(a). This can become significant for small field and/or wedged fields, since PDD is not following the central axis but drifting off axis under a different part of the wedge. For electrons, the effect can be dramatic for profiles at depths past d_{max}, especially for low energy electrons in which the percent depth dose curve is steep for the descending portion of the curve. Figure 7(b) shows the effect of tilting of the scanning arm on electron profiles.

III.B.3.c. Gantry tilt. A tilt in the gantry during data collection can have an effect on cross-plane profiles and/or depth dose data. The effect may be subtle such that, the scans may appear to be off center at deeper depths (Fig. 8). It is essential that the gantry be leveled prior to data collection.

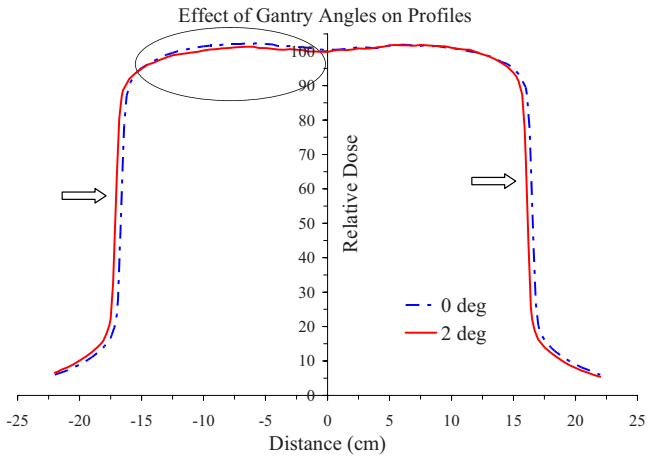

FIG. 8. Effect of gantry angle tilt on the profiles of a 6 MV beam for 30 $\times$30 cm^2 field at 10 cm depth.

The gantry angle should be checked with a precision level to avoid the appearance of asymmetry in the transverse scans.

III.C. Scan mechanism and movement

III.C.1. Array detector weight

In a water phantom system, the detector mount and scan mechanism are typically designed to support small, lightweight detectors. Some multidetector arrays may have a significant weight beyond the design of the scanning mount. Check with the scanner manufacturer before adapting a scanning system to use a detector array. Due to the size and weight of an array system, movement of the scanning arm should be checked before collecting data.

III.C.2. Speed and position accuracy

Depending on the detector signal strength, the sensitivity and/or sampling time of the scanning system electrometers, and the accuracy of positioning, there may be situations in which the scanning system cannot respond as fast as the scanning probe is moving. To test this, scan across 40 cm with a 20 cm field at the highest and lowest speed. Compare the two profiles for alignment. If the relative shape agrees but there is a shift, then there may be a limit as to how fast one can scan.

III.C.3. Hysteresis

A scanner should be tested for hysteresis in its position encoding. This is typically a problem with older scanning systems. They can be tested by scanning the same field at a moderate speed in one direction and then reverse the scanning direction. If these two profiles do not align and match perfectly, there is a hysteresis in the scanning movement. Such scanners should be sent to the scanning system manufacturer for repair and should not be used for scanning.

III.C.4. Corrosion

Follow the recommendations of the tank/scanner manufacturer on water additives, water storing, etc. Generally, it is

not advisable to let the scanning mechanism stay submerged when not in use for prolonged periods, especially overnight.

III.D. Premeasurement test

III.D.1. Dry run

The premeasurement tests should be performed for every new scanner before the first use of the tank before beam data commissioning. Also, it is essential to perform the test before an annual calibration which happens more often than the machine commissioning. After connecting all components but with no water in the tank, position the scanning detector at isocenter and the monitor detector at an appropriate position as to not to interfere with the scanning detector. A buildup cap may be used with the scanning detector. Perform an in-air scan of a 20×20 cm^2 field, allowing the scan to run from -20 to $+20$ cm (40 cm total). Make any necessary adjustments to the scanner's electrometer controls, as instructed in the manufacturer's user guide. A dry run may not work on some scanners that stop the scanning when there is no signal from the reference channel.

Repeat the scan; however, turn the beam off when the detector reaches the cross hairs. Save the scan and inspect the data either using the scanner's software or export it to a spreadsheet for analysis of the following items:

- Noise: In a flat region (slope of profile equals zero) of the profile, calculate the standard deviation. This is the standard deviation of the noise with the beam on.
- Signal-to-noise ratio: In the same region, calculate the coefficient of variation that is the standard deviation divided by the mean. This is closely related to the signal-to-noise ratio.
- Time constant: At the point where the beam turned off, examine the time it takes for the scan values to settle to the nonradiation value. This is related to the time constant (or response time) of the system, including any residual detector currents.
- Leakage: In the region after the nonradiation value settled to a flat value, calculate the mean and standard deviation of the nonradiation value.
- Electrometer offset: If there was no autorange changing of gain in the electrometer, the standard deviation in the nonirradiated area should be nearly equal to that calculated in the flat radiation region above. The mean value is the electrometer offset, which should be subtracted from all measurements (on the same gain).
- Polarity: If the electrometer is bipolar, there may be negative values and even a negative mean. This is normal and the subtraction of mean should preserve the sign, i.e., if a negative mean, then subtracting the negative value will actually add a positive value.
- Null value: If the nonradiation value (background) is zero and never changes, then it is possible that there is a suppressed zero in the data collection. This will result in a measurement error in penumbra and tail regions.

III.D.2. Water run

The cracks in the cable jacket or any leak in the detector may change the circuit parameters of the scanning device and possibly change the results when the tank is filled with water and the detector and cable is submerged. Do not submerge connectors unless they are known to be waterproof. After filling with water and submerging detector and cables, it is best to allow at least $\frac{1}{2}$ h or more to pass before proceeding with the test. Repeat the same tests as performed on the dry run and make sure that above parameters are nearly the same. The standard deviation of noise should not increase. Repeat the test again at the maximum scanning depth required. This will result in the lowest signal-to-noise ratio. This ratio should be greater than or equal to the known sensitivity of the system.

III.D.3. Saturation test

Repeat the above dry run procedure with an open 20×20 cm^2 field, at the maximum dose rate and a moderate dose rate. Compare the profiles.

III.D.4. Extracameral volume

Scanning detectors have a very small volume in the thimble where the ionization is measured. However, nonthimble area, connector, and cable irradiated either with scatter or primary radiation produce ionization contributing to the scan signal known as extracameral effect.[83,84,89] The extracameral volume is not constant since it does not originate within a chamber with good collection efficiency. After the saturation test, remove the scanning detector from its mount and place it on or near the electrometer. Start a scan and note the scanning detector response with and without beam on at the maximum dose rate. Any change in detector response is due to extracameral volume. It is assumed that the detector volume is significantly less than the extracameral volume. Compare this response with the signal from the tails of a profile measurement for its significance.

III.D.5. Energy response test

When performing PDD measurements with a diode, the energy response can be detected by comparing the measured PDD at 6 MV in a large (40×40 cm^2) field. Then repeat the measurement with a large volume scanning ion chamber. Compare the two PDD curves beyond $d_{\max}$. If the diode curve does not drop off as rapidly as the ion chamber PDD, then this is an indication of energy response variations. The large volume chamber (e.g., 0.6 cm^3) scanning should not be affected by stem leakage, assuming the chamber passes all other tests.

III.E. Data acquisition

Data acquisition should be conducted in an organized fashion to avoid confusion. The order of scan acquisition on many scanning systems will greatly improve the ability to access the scan data later. In addition, the data should be acquired such that sets of data can be collected at the same

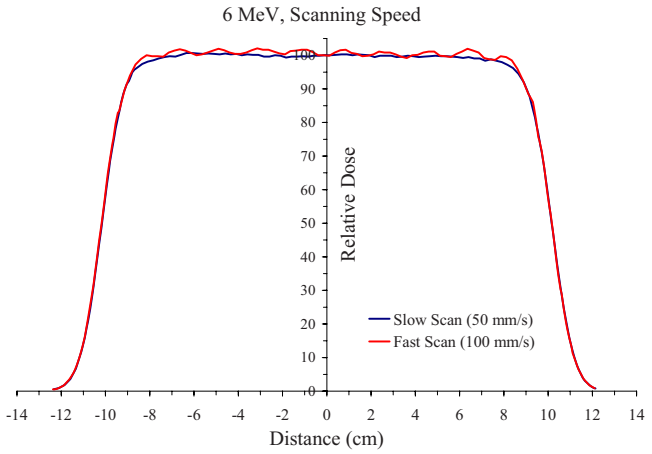

FIG. 9. Impact of scanning speed on the quality of electron profile.

time to improve the consistency and accuracy of beam data. Organization of the measurements needed with a spreadsheet as shown in Table I, will be helpful in expediting the data collection.

III.E.1. Scanning parameter protocol

Data collection has several components that depend on the software being used. However, one should utilize the features of the scanning software for optimum management and quality of data which depends on speed, time delay, and sampling time. As discussed in Sec. I B 4, a significant amount of time is needed to commission beam data. There is a tendency to reduce the overall scanning time, as noted in Eq. (1), by increasing scanning speed and sampling data coarsely. Speeding and undersampling produce suboptimal data especially for low energy electron beams. These will be discussed in their respective sections.

III.E.2. Speed

High scanning speed can result in noisy scans and/or ripples in the acquired data due to wave motion induced by the movement of the scanning arm. This is especially critical for profile acquisition at depths greater than d_{max} for low energy electrons. If the motion is too fast, the wave motion induced will cause the scanning probe to see a varying depth depending on whether at the peak or valley of the water wave. Figure 9 illustrates this effect for profiles but it is also observed in PDD data with wavy curves. Scanning speed can also be critical for a small field in which a small volume ion chamber is being utilized. Due to the small signal, slower scan speeds will be required to help smooth out the statistical variation in the chamber signal.

III.E.3. Delay time

A delay time is introduced between measurements at two consecutive points. Longer delay time can increase data collection time but it is certainly advantageous for electron beam scanning since small ripples in water could change the data significantly.

III.E.4. Sampling time and signal

Sampling time is the time when the detector is stationary as data are being collected. The sampling time should be long enough based on the gain of the electrometer and the size of the detector (amount of signal). Before collecting data, one should check this in the penumbra region at the deepest depth and choose the appropriate sampling time. It is also advisable to check the impact of these parameters over the allocated time for commissioning.

III.E.5. Radio frequency noise interference

There is no radio frequency interference with the detector signal when conductive shielding of the entire measurement system: the shell of the chamber or diode, the cable outer braid shield, connector adapters, the electrometer connector, and the electrometer chassis, are intact. A simple conductive shield test could be performed with electrostatic charges in a dry (not humid) environment by simply shuffling of shoes on the floor and waving hands over the proximity of the components. In addition, touching the components and looking for a change in measurement response may reveal possible connection problems.

III.F. Data file

III.F.1. Data file organization

For easy data retrieval, the photon and electron beam data should be placed in separate folders with different identifiers. Furthermore, the user could subdivide photon data into open and wedged beam folders. With a good file organization, the user saves a lot of time retrieving specific data from a huge number of data files.

III.F.2. File name

As data are acquired, a file name convention should be established to assist data retrieval for later times. For many scanning systems, the file name is automatically assigned or is limited to eight characters, which greatly complicates the file naming convention process. If the file name is limited to eight characters, creativity is required to eliminate confusion and/or duplicate names. An example of a naming convention would be energy, open or wedge, and type of scan, e.g., 6P15WDD. Even if there is only a Windows type limit to the file name, a naming convention should be adopted to eliminate confusion later, such as "6 MV open depth dose set" or "18 MV 15 deg wedge 10×10 profiles." In some older systems, data files are internally managed in a single file. In such a situation, detail comments of each scan should be saved which will help in data retrieval and analysis.

IV. PHOTON BEAM DATA

IV.A. Photon scanned data measurements

The scope of data measurements will depend on the requirements of the user's dose calculation systems (e.g., TPS, monitor unit calculation system, etc.). Additional data may be measured to confirm the accuracy of the planning system

for specific treatment setups.[2] All of these data may be acquired either using beam scanning systems or point dose measurements (nonscanned data). Scanning systems are used to measure the characteristics of the beam when the parameters defining the beam are fixed. The variation of dose with depth (i.e., PDD) and off-axis position is determined by sampling the beam at different positions. The nonscanned measurements are usually performed in cases where the parameters defining the beam [e.g., field size, SSD, presence of ancillary device(s), etc.] are varied. In these cases, the output change is usually measured at a single normalization depth, so that fewer data are typically required. A spreadsheet might be helpful in organizing the amount of data to be taken as shown in Table I. Such a table also provides a place to write the name of the file when data are collected.

IV.A.1. Depth dose

The PDD measurements are taken with a fixed SSD customarily at 100 cm distance, which is typically the isocenter for most modern linear accelerators. During acceptance testing, PDD is often taken with a limited scatter device, such as the Wellhofer Buddelschif or PTW system used by the linear accelerator installer to match the beam parameters provided from the factory. It is recommended that these data should not be used for commissioning the machine. Other precautions, as mentioned earlier, regarding speed, step, gain, etc., should be followed. It is a good practice to start depth dose from the bottom of the tank rather than from the top as it minimizes the wake and disturbance in the water.

IV.A.1.a. Standard and nonstandard SSD. Normally, data should be taken as close as possible to the conditions pertinent to most clinical situations, so as not to introduce errors through auxiliary scaling operations. With a calibration depth at 10 cm, the natural SSD to represent isocentric conditions is 90 cm. Hence, the natural specification for TPS commissioning for isocentric cases would be 90 cm. However, TPS vendors might have specified 100 cm SSD for beam commissioning since there is a long tradition of such setup. Additionally, some of the current protocols for beam calibration require PDD data measured at 100 cm SSD. Independent of the SSD, the ability to model correctly the dose at any SSD should be checked as part of the beam commissioning.

Scaling of data taken from a different SSD should only be used as QA checks to ensure consistency, rather than to circumvent the need to acquire data for the specified SSD. For photon beams, several phenomena render a simple SSD correction inadequate since different components scale differently with SSD:

- Electron contamination: The surface dose and buildup region are associated with the complex behavior of electron contamination. They depend on various factors including field size, beam energy, SSD, beam modifying devices, angle of the beam, etc.[90–101] Electron contamination cannot be generally scaled by any SSD except that it can be minimized with proper techniques adopted by the manufacturer.[102,103] The relative amount of electron contamination changes with the length of the air column (standard versus extended SSD) as head scattered electrons decrease with increased scattering in air.
- Primary dose: It is well behaved and can be scaled for different SSDs just by applying the inverse square law, except for small field sizes close to what is required for lateral electron equilibrium. For such small fields, the variation of field size with depths may change the equilibrium level in a nonscalable way.
- Scatter dose: Larger projected field sizes contribute more scatter which is the main cause of the difference remaining between PDDs (at depths beyond the maximum depth of electron contamination) for different SSDs while removing the inverse square factors.
- Head scatter: It scales primarily by inverse square to the dominant source, i.e., the flattening filter. The effective center for head scattered photons is close to the flattening filter, thus the inverse square factor is different for the direct and head scattered beam components. This will imply different results both for PDD (different mix of direct to head scatter) and transversal beam profiles (the head scatter field goes outside the direct beam).
- Energy: The off axis softening is driven by the off axis angle so scatter factors for the same field size defined at the surface for different SSD will be generated with slightly different effective spectra.
- Penumbra: It cannot be scaled from one SSD to another when scanning with a chamber that has a significant spread function. If small dimension detector is not available profiles could be deconvoluted, as discussed in Sec. IV A.

For simple QA purposes, an inverse square factor could be used to scale between small differences in SSD (small field warning, see above), but otherwise the above recommendations regarding measurements should be followed.

IV.A.1.b. Conversion between PDD taken at different SSD. Percentage depth dose is often used for fixed SSD treatment and for determining other depth dose data, e.g., TPR. The PDD is customarily measured at 100 cm SSD. However, it can be measured at any distance such as SSD=90 cm. The advantage of a shorter SSD is the ease of phantom setup for coverage of large field sizes. However, PDD is a function of SSD in addition to field size (s) and depth (d). One can derive the relationship for PDD measured at different SSD as described in various references.[88,104]

IV.A.1.c. Extended distance (>100 cm) *beam data (TBI, TSEI).* For special procedures like total body irradiation, total skin electron irradiation beam data such as depth dose, TPR or TMR, profiles, should be collected at the extended distances as described by specific AAPM report.[23,24] Such data are difficult to collect due to the tank size limitation. If such data are collected they should be verified against point measurements in a large phantom.

IV.A.2. Tissue maximum or phantom ratio, TMR/TPR

TMR data are often difficult and time consuming to measure. There are water phantom systems that collect TMR/

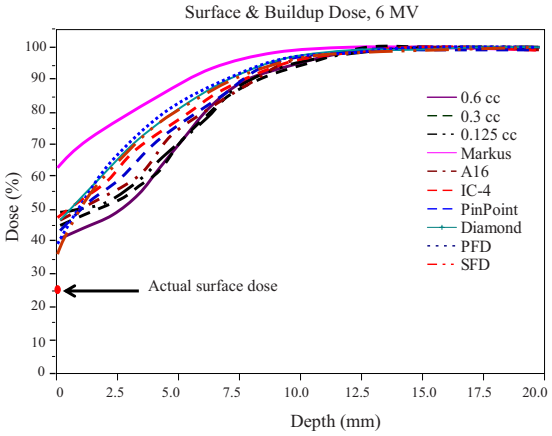

FIG. 10. Surface and buildup dose for 10×10 cm^2 field of a 6 MV beam with various detectors. The actual surface dose is also marked by the arrow.

TPR data by pumping a known amount of water for measurements at each depth. Such measurements are time consuming and the accuracy needs to be verified by independent point measurements. The simplest approach is creating TMR/TPR from depth dose measurements. Most software rely on the BJR Supplement 25 (Ref. 104) approaches (described by Khan[88]) and have built-in conversion processes. TMR at a depth d and field size r_d can be calculated from the PDD measurement as shown below

$$\mathrm{TMR}(d,r_d) = \frac{\mathrm{PDD}(c,d_r,\mathrm{SSD})}{100}\cdot\frac{(\mathrm{SSD}+d)^2}{(\mathrm{SSD}+d_{\max})^2}\cdot\frac{S_p(r,c_{d\,\max})}{S_p(r,c_d)}. \quad (2)$$

TMR values created from the above equations should be carefully verified especially at extreme field sizes and deeper depths. To create these tables, interpolation of the PDD is needed, and hence for small field TMRs, relatively smaller field PDDs are needed. When vendor provided software is used to convert the PDD to TMR, one should be extremely careful to check the calculation at small fields and deeper depths since extrapolation might result in poor results. Point measurements are recommended to check the validity of these conversions.

IV.A.3. Surface dose and buildup region

The surface dose is machine dependent, and can be affected by many parameters, including the field size, the source to surface distance, the presence of beam modifiers, and the angle of beam incidence.[97,105–115] The commissioning of an accelerator normally includes the measurement of surface dose. Because of the steep dose gradient near the surface as well as in the buildup region, careful considerations are required in the selection of detectors.[115–118] Figure 10 shows the buildup and surface dose taken with different detectors. Generally, the size of the detector along the beam direction should be as small as possible. It is highly recommended that the surface dose measurements should not be made with a scanning device.

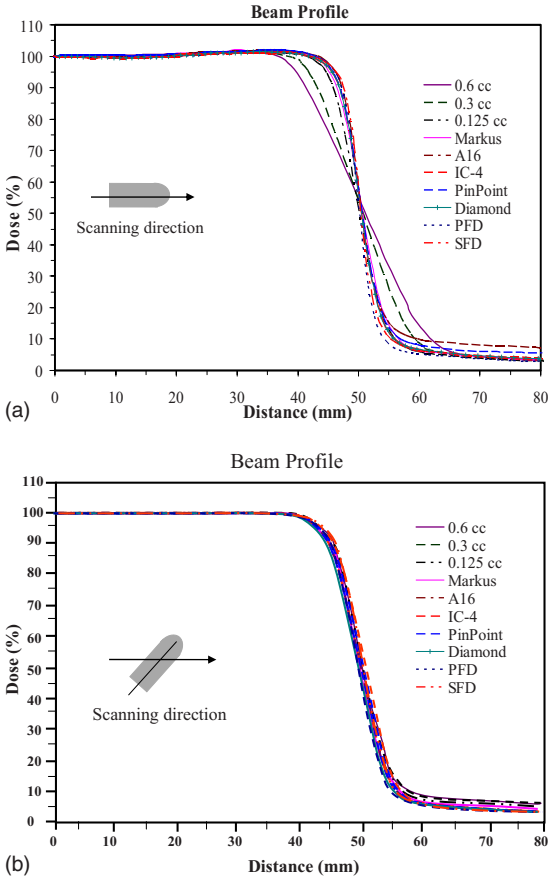

FIG. 11. Effect of chamber orientation on photon beam profiles for a 10 $\times$10 cm^2 fields: (a) long axis scan, (b) short axis scan with various size detectors. Only half scans are shown.

Extrapolation chambers are the detectors of choice for surface dose. However, its availability is limited and its use in surface dose measurements is very time consuming. Instead, fixed-separation plane-parallel chambers are commonly used for surface dose and the dose in the buildup region. Because of their relative large separation compared with the extrapolation chamber and their small guard ring, the plane-parallel chambers show an over-response in the buildup region and especially at the surface.[90,119] The inaccuracy may be reduced by using chambers with a small plate separation and wide guard ring. Furthermore, the chambers may exhibit a polarity effect,[90] which may be corrected by averaging the readings obtained with positive and negative polarities. Measurements of the surface dose by thin layer of TLD, diode of small active volume, MOSFET, or radiochromic film have also been reported.[117,120,121]

IV.A.4. Beam profiles

IV.A.4.a. Profiles (penumbra and off axis factors). The choice of detector orientation is critical for profile measurements for small fields and high gradient regions. The proper detector and detector orientation should be maintained when measuring a profile, as shown in Fig. 11, for relatively large fields. Figure 11(a) demonstrates the effect of chamber volume averaging when measuring a field profile and clearly

indicates that a small volume detector is preferred for profiles. Orientation and data collection, as shown in Fig. 11(b), should be used. In general, both in-plane (gun-target) and cross-plane (left-right) profiles are needed for commissioning. If there is an option to choose between in-plane and cross-plane, cross-plane profiles should be acquired since steering of the electrons in some machines is only possible in gun-target direction and prone for asymmetry and loss of flatness over a period of time. The profiles in cross-planes are usually stable and should be the choice of the direction for the data collection.

Dose profiles are collected during commissioning for input into the treatment planning computer and for additional monitor unit calculations with either manual method or commercial computer software. The profile requirements depend on the TPS; however, most TPS require profiles from very small fields to the largest field size available in order to model the penumbra and off axis factors for the open and wedged fields. The data should be collected with a maximum of 1 mm spacing in the penumbra region and preferably no more than 2 mm spacing in the remainder of the field. In converting profile data to an off-axis table, each profile needs to be renormalized to the central axis value and scaled to the distance at isocenter. Many scanning systems provide software to facilitate the process.

The number of profiles, in terms of field size and depths, are dependent on the TPS. The numbers of profiles do not need to be excessive since the basic shape of the beam does not change dramatically with depth and/or field size. Typically, profiles at 5–7 depths are sufficient for each 1 cm spaced field size up to 6×6 cm^2, and then 5 cm spacing for field sizes 10×10 cm^2 and greater is sufficient. A spacing of 5 cm with depth, with the inclusion of $d_{\max}$ profile, is usually sufficient. Some TPS require in-plane, cross-plan, and diagonal profiles and for those systems all of the required profiles should be taken.

IV.A.4.b. Star patterns. Some TPS algorithms may require beam profiles at several angles with respect to the collimator axes in a given plane. Such profiles are called star patterns typically taken at 10° interval and at $d_{\max}$ or 10 cm depth for the largest field size. Some water scanning systems have built-in software to collect the star patterns diagonally at certain angles. If such software is not available, the star pattern should be taken manually by rotating the tank on the machine pedestal at certain angular intervals, typically 10°. Star patterns provide a knowledge of the beam characteristics representative of the flattening filter.[122] The star pattern scan should never be acquired by rotating the collimator, as it does not provide the shape of flattening filter.

IV.A.4.c. Physical or hard wedge. The profiles are generally taken in the wedge direction similar to open beam and as outlined in Table I(a). Care should be taken to collect data at smaller spacing in high gradient area. Physical wedges attenuate beam in both the gradient and nongradient directions of the wedge. For large fields data should also be taken in the nongradient direction to examine the impact of rounding off, as shown by various authors,[123,124] due to oblique incidence of the beam and selectively higher attenuation at off axis.

IV.A.4.d. Soft or electronic wedge. Soft or electronic wedge (dynamic or virtual wedge) profiles require different type of data collection equipment than the standard scanning system. Since the soft wedges are formed by the moving machine jaws while the beam is on. The standard scanning system utilizing a single chamber cannot be used to collect such wedge profiles. The types of detector systems such as films and linear detector arrays (ion chamber or diode) which can be mounted on the scanning arm[44,45,59] have been used, since all the measurements are being made in water under conditions of full scatter. However, the numbers of scanning systems that offer this option are limited and the cost for a one-time application may be difficult to justify for some institutions. Another option is to use a diode array, such as the profiler (Sun Nuclear, Melbourne, FL) with different thickness of solid or virtual water slabs to achieve various thickness up to at least 20 cm. These diode arrays have been shown[45] to give good agreement with water scans and in most cases, commercial software exists to convert the diode array profiles to a format which the treatment planning computer can read. However, the profiler is limited in the maximum field size that can be measured. Another option is to use film dosimetry with a film sandwiched between slabs of solid or virtual water, and imaging software for analysis. With film dosimetry, the film must be calibrated to generate a density vs. dose response curve. A good QA on the film processor is also required. A problem with film dosimetry is its spectral dependence of the sensitometric curve.[21] Film size limitation is another problem that should be considered.

IV.B. MLC data

MLC is now an integral part of a linear accelerator and is available in various sizes (regular, mini, and micro) that have been developed for specific uses depending upon the leaf widths. The mechanical stability and characteristics should be known and verified during the acceptance testing of the machine which has been reported for various manufacturers.[125–145] In general, MLC commissioning data depend on the clinical usage but more importantly on the TPS. Detail discussions on the various MLC designs and their commissioning had been provided by the AAPM Report 72 (Ref. 145) and IPEM Report 94.[16] However, some of the parameters, as described below, should be quantified for each photon energy and a minimum of four gantry angles (0°, 90°, 180°, 270°) to examine the effect of gravity on leaf motion.[146,147]

- Light and radiation field congruence
- Interleaf leakage (leakage between two leaves)
- Intraleaf leakage (transmission though a leaf)
- Tongue and Grove effect across the field
- Penumbra.

In addition, positional accuracy critical in dosimetry[148] may be determined either with film or electronic portal imagers.[147,149] For MLC with curved end leafs, an offset for the leafs positioning should be determined to account for the fact that the 50% isodose line is not at the tip of the curved ends.[141] Except penumbra, all these parameters should be

acquired using film dosimetry. Inter- and intraleaf leakage could be measured with a well calibrated film or portal imager that provides high resolution data. For MLC with backup jaws, the data should be acquired with jaws retracted. A reference film at a reference depth should be exposed that provide correlation between optical density and dose. The MLC leaves should be closed with the non-MLC jaws retracted to fully open positions. A large film that covers the entire MLC leaves should be exposed. If the film is small compared to the MLC field size, SSD could be decreased. This will help reduction in MU which is typically 10–20 times the reference MU. After processing the film, it should be scanned and proper correction factors should be applied to convert optical density to dose to quantify the inter- and intraleaf leakage. These values should be compared with published data in the literatures[150] for the type of manufacturer.

IV.C. Photon point dose data

The data required by TPS vary considerably from one system to the other. However, at least for manual dosimetry calculations, the following data should be collected.

IV.C.1. Total scatter factor (S_{cp})

The relative output from a treatment machine is defined as the dose for a given field in water relative to the same quantity in a reference geometry, which usually is the reference depth and field size. The total scatter factor, S_{cp}, is defined as the ratio of the dose for the same monitor units (M) for the field of interest to the dose for the reference field, both measured in a large water phantom with the detector at a reference depth at the isocenter

$$S_{cp}(s) \equiv \frac{D(s,d_{\text{ref}})/M}{D(s_{\text{ref}},d_{\text{ref}})/M}, \tag{3}$$

where D is the dose measured in phantom, in this case at the reference depth d_{ref}, and for the field size, s, and the reference field size, s_{ref}, and M is the monitor unit. The use of a large water phantom ensures that full lateral buildup is established for the field in question. The depth of water beyond the deepest point of measurement in the phantom should be at least 10 cm to ensure full backscatter. It should be noted that the values determined at depth (e.g., 10 cm) will be significantly different from the values determined at $d_{\max}$, thus it is important to know what data is required before proceeding.

IV.C.1.a. Measurements. Relative output should be measured in water at a defined reference point (e.g., at 10 cm or $d_{\max}$), 100 cm SSD or SAD for a variety of field sizes as shown in Table I. Ideally, the data should be collected in the same manner as the machine is calibrated, i.e., SSD or SAD calibration. If IMRT data are required, the relative output in water should be measured with a small volume chamber for small field sizes. The chamber dimension must be small compared to the smallest field size, e.g., less than 0.5 cm in any dimension (diameter or length) to avoid chamber averaging effects. It is suggested that these data can be compared to data collected with a larger chamber for larger field sizes to see if the data overlap and form a smooth curve of S_{cp} versus field size. On occasion, the small volume chamber may exhibit significant stem effect or effect of cable irradiation for the reference 10×10 cm^2 field. Also, it is known that the readings for $\leqslant 3\times3$ cm^2 field may have chamber volume averaging effects and consequently the readings may be 5–10% lower than the true value, depending on precision of chamber positioning and beam profile.[151–153]

IV.C.1.b. Monte Carlo approaches. It has been proven that the Monte Carlo method can precisely model the physical processes involved in radiation therapy and is powerful in dealing with any complex geometry.[154–156] In principle, the Monte Carlo technique can produce accurate dose calculations, under almost all circumstances, provided that relevant phase space data are available and the calculations have been benchmarked appropriately. By simulating the detailed accelerator head geometry, Monte Carlo techniques can provide accurate information about the particles emerging from each component of the accelerator head, which can be used to characterize the beams.[157–159] In particular, Monte Carlo studies have been carried out to (1) determine the relative scatter factors, (2) analyze the various components of the scatter factor, and (3) designs new methods to measure the scatter factor.[10,11,13] For example, Monte Carlo simulations have shown that scatter contributions from collimators (such as jaws and MLC leaves) are significant for small fields.[160–162] Monte Carlo approaches have been introduced for either validating the measurements or generating the small-field data.[13,153,163,164]

IV.C.2. In-air output ratio (S_c)

This quantity is also called in-air output factor,[165] collimator-scatter factor,[88] or head scatter factor.[166,167] The latter two names were somewhat misleading since they emphasized a single component of the output ratio. The TG-74 (Ref. 20) report describes the details of the in-air output ratio, S_c, and defines it as the ratio of primary collision water KERMA in free-space, K_p, per monitor unit (M) between an arbitrary collimator setting and the reference collimator setting at the same location

$$S_c \equiv \frac{K_p(c;z_{\text{ref}})/M}{K_p(c_{\text{ref}};z_{\text{ref}})/M}, \tag{4}$$

where c is the arbitrary collimator setting, c_{ref} is the reference collimator setting, usually 10×10 cm^2, and z_{ref} is the reference source-to-detector distance, usually 100 cm. Notice that the primary collision kerma excludes the scattered collision kerma generated in any surrounding phantom but includes all scattering that has occurred in the treatment head.

Experimentally, S_c can be determined as the ionization ratio measured in a miniphantom with sufficient thickness to eliminate electron contamination.[32] The lateral dimensions of the miniphantom should provide lateral electronic equilibrium at the detector, as well as filter contaminant electrons from the side. The material composition of the miniphantom

must be carefully chosen so that significant medium-based deviations in water kerma ratios due to spectral differences between beam c and c_{ref} are not introduced. However, in situations when the beam quality is different from reference conditions (e.g., while using physical wedges), it has to be noted that S_c, as an estimator of the energy fluence ratio, is biased by the collision kerma and attenuation at measurement depth.

Traditionally, S_c is measured using an ion chamber with a buildup cap. The selection of buildup cap is very important. It is better to err on the side of excess buildup material than too little. If the buildup cap is not of sufficient thickness, the chamber will respond not only to the electrons generated by photon interactions in the cap, but also to the electron contamination in the beam, which can produce erroneous results. The reader is referred to the report from TG-74 for the appropriate dimensions of the buildup cap. The indication of insufficient buildup cap thickness is the presence of pronounced in-air scatter ratio (S_c) with field size, which in turn will cause the calculated phantom scatter factors (S_p) to become flat with field size. For small field sizes ($\leqslant 4\times 4$ cm^2) extended distance can be employed if one has to use the same water-equivalent miniphantom. It is important also to measure the output factor at 10×10 cm^2 at an extended distance so that the two sets of output factors measured at different SSDs can be merged. TG-74 recommends using high-Z miniphantom and making the measurement at the same SSD as those for other field sizes ($>4\times 4$ cm^2). The minimum field size is determined by the requirement that there is sufficient "flash" of at least 1.0 cm around the miniphantom.

IV.C.3. Phantom scatter factor (S_p)

The phantom scatter factor, S_p, is defined as the ratio of the scatter factors between the actual field size, s, in the phantom and that of the reference field size, s_{ref}, both at the reference depth, d_{ref},

$$S_p(s) \equiv \frac{SF(s,d_{\mathrm{ref}})}{SF(s_{\mathrm{ref}},d_{\mathrm{ref}})}, \tag{5}$$

where SF is the ratio of the total dose in water (D) to the primary dose (D_p) for the same field size and depth at the same location. The phantom scatter factor can be approximately determined by

$$S_p(s) \approx \frac{S_{cp}}{S_c}. \tag{6}$$

In deriving S_p in Eq. (6), we have used Eqs. (3) and (4) which define S_{cp} and S_c, respectively. Using the primary dose-to-collision kerma ratio, β_p, one can relate the primary dose $D_p=\beta_p\cdot K_p$, to the primary water collision kerma. Equation (6) holds exactly if the primary dose-to-kerma ratio is field size independent: $\beta_p(s)=\beta_p(s_{\mathrm{ref}})$.

IV.C.4. Wedge factors

IV.C.4.a. Physical wedge. Generally, a wedge factor is a function of wedge angle, depth, x-ray energy, and field size as noted by various authors.[168–173] Hard or physical wedge factors should be measured at the reference depth (10 cm or d_{max}), 100 cm SSD for different field sizes. For some accelerators, the wedge factor is a strong function of field size, for which a larger range of field sizes should be included in the measurement.[170,171,174] Most planning systems allow the user to specify the particular field sizes for wedge factors.

Due to the inaccuracy of placing the detector at the exact beam center, it is necessary to first center the chamber in the beam, with detector axis along nonwedged direction by taking readings with a 60° wedge at two collimator angles (180° apart). Once the detector is centered in the beam, one must acquire readings at one wedge orientation and then repeat the measurements with the wedge reversed 180 deg. The wedge factor is taken as the average of the two wedge orientation readings divided by the open field reading at a single collimator angle. The wedge factor measured at depth can be significantly different from the wedge factor measured at d_{max}. Typically, the TPS will dictate the depth of measurements for wedge factors. However, for manual dosimetry tables in which both open field and wedged field PDD and TMR tables are present, it may be appropriate to use wedge factors measured at d_{max} to avoid correcting for beam hardening twice. When two sets of physical wedges are available, for example Varian's lower and upper wedges, data need to be verified. It is advisable to spot check the wedge factors for field size and depth; however, Cheng *et al.*[175] found that wedge factors are nearly identical for lower and upper wedges.

IV.C.4.b. Soft wedge. Soft wedges are electronic wedges or nonphysical wedges known as dynamic or virtual wedges that vary in operation depending upon the manufacturer. Enhanced dynamic wedge (EDW) is used by Varian, while the virtual wedge (VW) is used by Siemens.[176–179] Both vendors utilize the movement of one Y-jaw to simulate a wedge, while keeping the other Y-jaw stationary. The major difference between EDW and VW is that for EDW, both the jaw speed and the dose rate are variables, while in VW, the jaw speed is constant and the dose rate varies according to an analytical function.

The wedge factors for these different types of electronic wedges can be quite different from physical hard wedge factors. The wedge factors for the EDW, defined at a depth of 10 cm at the center of the open field, exhibit field size, and wedge angle dependency, with values 10%–30% higher than the corresponding physical wedges. Studies have shown that the wedge factors for the EDW are independent of depth because the beam quality is not changed by these wedges.[175,180] By contrast, the Siemens virtual wedge factors exhibit values of $1.0\% \pm 2\%$ with no observable relationship between wedge factors and field size or wedge angle. Wedge factors should be measured at the reference depth as specified by the vendor (10 cm or d_{max}) at 100 cm SSD or SAD for different field sizes. Additional wedge factors for rectangular field should be measured since wedge factor seems to have a greater dependence on the moving jaw dimension than the fixed jaw position. For example, Varian EDW wedge

factor for 10×20 cm^2 will have a value very similar to the wedge factor for 10×10 cm^2, a phenomenon that is not present with physical wedges.

IV.C.4.c. Universal wedge. Elekta accelerators use the combination of an open field and a built-in 60° physical wedge to achieve different wedge angles by software control. The wedge is motorized so that it can be moved in and out of the field. This type of wedge system is known as an internal or universal wedge. The wedge factor should be measured for various field sizes and at various depths, as required by various TPS and described in various publications.[181–184]

IV.C.5. Tray factors

Transmission factors for blocking trays, jaws, and MLC are measured at reference depth (10 cm or d_{max}) in water,[185] and are defined as the ratio of the reading with the blocking tray or jaw or MLC bank to the reading for the same point in the open field. Due to the small transmission through the jaws and/or MLC bank, a large monitor unit setting is often required to ensure readings are collected in the linear range of the electrometer/detector system and to ensure good statistics. Tray transmission factors may also be measured without a water phantom system.

IV.C.6. Small field considerations

Traditionally, fields in radiation therapy span from 4×4 cm^2 up to 40×40 cm^2. However, in advanced and specialized radiation treatments, such as IMRT, SRS, CyberKnife, and gamma-knife, extremely small fields of the order of few millimeters are used. A detailed list of problem and future trend in the dosimetry of small field has been described by Das *et al.*[152] Small-field dosimetry is challenging due to lack of lateral electronic equilibrium,[186] overlap of the geometrical penumbra due to the size of detector,[152] change in energy spectrum and associated dosimetric parameters, and stopping power ratio.[163,187–189] Several problems and trends in the dosimetry of small field have been covered in some detail by several authors.[11,13,64,66,67,151,152,163,164,187–202]

Small volume detectors should be used that have minimum energy, dose, and dose rate dependency. Microion chambers are best suited for small field dosimetry; however, their signal-to-noise issue should be evaluated. Additionally, perturbation factor of these detectors should be taken into account, as shown by Sauer *et al.*[164] and Francescon *et al.*[153] If a scan through the field center varies more than 1% over the range of the detector diameter, consider changing to a smaller detector. Output factors are very sensitive to the position of the detector. Thus, verification of centering of the detector is important.[151,202] This could be performed by scanning across the field in both lateral dimensions to check that the maximum along each dimension coincide. A more elaborate method has recently been proposed by Li *et al.*[203] The actual field size used during the output measurements should also be verified, since a small error in the field size setting will produce a large error in the output. However, the full width at half maximum estimated from (correctly measured) profiles for fields where lateral disequilibrium prevails will not yield the correct field sizes. They will overestimate the field size since the half maximum is now located at lower dose levels, i.e., closer to the toe end of the profile as the maximum is less than the equilibrium value. An independent check and calibration of the light field, or shifting position of the leaves, might provide a means for field edge location checks.

V. ELECTRON BEAM

V.A. Electron scanned data measurements

V.A.1. Depth dose

Electron beam depth doses differ significantly among institutions and manufacturers as shown by Followill *et al.*[204] It is therefore recommended that each electron beam data should be measured during commissioning. Diode detector, parallel plate ion chamber, cylindrical ion chamber, and films are the most commonly used detectors in electron beam scanning. It is extremely critical to establish the correct zero depth to obtain good percent depth dose data. For cylindrical ion chambers, 0.5 radius shift for the point of measurement relative to the chamber center can be used.[56,145] A quick depth ionization scan for a low energy (e.g., 6 MeV) electron beam can be used to check if the zero depth is set correctly. The resultant curve will have a well-defined d_{max}, with an average value of 1.1 ± 0.2 cm for 6 MeV, regardless of the vendors. A measured ionization d_{max} outside of this range by more than 0.2 cm may indicate an error in establishing zero depth. Percent depth ionization curves should be scanned for all energies for the reference cone to a depth of R_p+10 cm with depth increment of 0.1 cm. In electron beam commissioning, the 10×10 cm^2 or 15×15 cm^2 cones are commonly chosen as the reference cone. From these percent depth ionization curves, the following depths: d_{max}, d_{90}, d_{80}, d_{70}, d_{60}, d_{50}, d_{40}, d_{30}, d_{20}, and R_p can be determined to define the depths of the profile scans. Note that strictly speaking, R_p should be determined from the depth dose data corrected for beam divergence. However, for SSD$\geqslant$100 cm, the difference in R_p obtained from depth ionization data is not clinically significant from that determined from the depth dose data.

When an ionization chamber is used for measuring depth ionization curves in a water phantom the readings should be converted to the corresponding depth dose curves using the appropriate replacement correction factors and restricted stopping power ratios. Most scanning systems have built-in software to convert ionization to dose. However, the accuracy of the conversion must be verified at selected positions based on the data provided in the references.[22,56,88,205]

Scanning speed, delay time, and sampling time as described in Sec. III should be properly evaluated for electron beam scanning as these parameters impact the quality of the scan. Figure 12 shows the effect of water ripple on an electron depth dose curve. Any abnormal depth dose characteristics should be investigated in terms of scanning parameters. The ideal detector for electron beam scanning is a small vol-

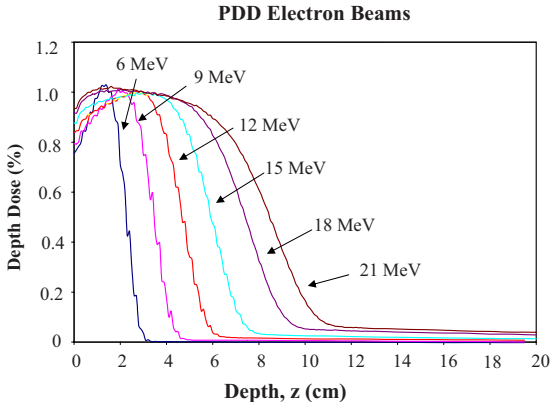

FIG. 12. Effect of water ripple on low energy electron beam depth dose.

ume electron diode since it does not require an ionization reading to dose conversion and there is no shift in its position except for a small amount of waterproof coating on the top the detector; typically ~0.2 mm.

For some TPS, accurate knowledge of bremsstrahlung radiation is important. The component of bremsstrahlung radiation can be accurately acquired by the method described by Zhu *et al.*[206] In this method, bremsstrahlung is divided into three components (head, cerrobend, and water) and measured by eliminating different components. If the PDD for an electron cutout is measured with an electron diode, the bremsstrahlung component is usually inaccurate since electron diodes do not respond accurately to photons.

V.A.2. Profiles

While dose profiles are typically measured at various depths such as d_{max}, d_{90}, d_{70}, d_{50}, d_{30}, and d_{10}, i.e., depths at 100%, 90%, 70%, 50%, 30%, and 10% dose, respectively, but may vary depending on the specification of the planning system. When collecting profile scans, attention should be given to the profiles at depths greater than d_{max}, especially for the low energy electrons. If a pronounced asymmetry is observed in the profiles, the leveling of the tank and/or scanning arm and accuracy of gantry angle should be rechecked. With low energy electron, it is common to see "ragged" scans, especially at large depths. Several factors should be examined: the gain of electrometer, placement of the reference probe, the direction of scan motion, the probe motion rate, and/or sampling time, and/or repetition rate on machine to see if the scans could be improved. For some linear accelerators, the profiles could be improved also by turning off the dose servo; however, it should be verified also in clinical mode. For certain scanning systems, the profiles could be improved by readjusting the autogain setting and background. Yet, for some linear accelerators, the only solution appears to be slowing down the scan rate and increasing the sampling time as beam profiles are very sensitive to scanning speed for low energy beams and at deeper depths as shown in Fig. 9.

V.B. Electron point dose data

V.B.1. Cone factors

Cone output factors are defined as the ratio of dose at d_{max} for a given cone to the dose at d_{max} for the reference cone; typically 10×10 cm^2 or 15×15 cm^2. Cone factors should be measured in a water tank or in solid phantom with size $\geqslant30\times30$ cm^2 if the output of the 25×25 cm^2 cone is measured. Different machines of the same make and model may have different cone output factors (e.g., the cone output factors may be different for two different 21EX machines), although the difference may not be large, e.g., $<2\%$. It is recommended to verify cone factors of all cones for all energies to confirm if the cone factors of one machine can be used for the other machine of the same model.

V.B.2. Cutout factors

A cutout factor is the ratio of the dose with and without the cutout for a given cone measured at their respective d_{max} depths. It is useful to prepare a table of cutout factors as a function of energy for standard cutouts for clinical applications where the respective d_{max} is specified. Cutout shapes include rectangles, circles, ellipses, and squares. The standard cutout output factors are usually tabulated versus their equivalent squares. The calculation of equivalent squares and output for electron beams is discussed in various references.[22,56,205,207] For very small cutouts (e.g., 1×2 or 2×2 cm^2), the d_{max} may be different from that of a larger cutout and should be determined for the cutout measurement. The choice of ion chamber and its placement for small cutouts are critical. Cutout factors at extended distance (e.g., 110 cm SSD) may be determined by measurement, or by calculation, using the virtual SSD determined for a set of standard cutouts during machine commissioning and the cutout factor at 100 cm SSD. Agreement within 2% can be achieved between the two methods. There are several methods listed in the literature[208,209] that use a sector integration technique similar to the Clarkson method to predict cutout output (dose/MU) for any irregular cutout at any SSD with accuracy within $\pm2\%$.

V.B.3. Virtual and effective source position

Due to electron scattering through various materials in its path, electron beams do not follow a strict inverse square law. In particular, a high abundance of indirect radiation scattered from collimators and cones are not amenable to characterization by a single source.[210] For beam characterization, there are empirical approaches to solve this problem by determining the source position that would allow the use of inverse square law.[56] The gap method and σ_{θ_x} method[205,211] have been suggested for the estimation of the virtual source. The gap or effective SSD method, as described by Khan[88], allows the user to use the inverse square law to calculate electron dose at any distance. This method is relatively simple and requires the determination of the effective SSD for electron beams, which depends on the machine, field size, and beam energy.[212–216] By taking measurements at d_{max}

at various air gaps between the electron cone and water surface, a plot of the square root of I_0/I and the gap gives a straight line with a particular slope that provides the effective SSD. Sigma-theta-χ (σ_{θ_x}) is the root-mean-square value of the Gaussian projected angular distribution at the plane of the final collimating device as described by ICRU-35 (Ref. 205) and van Battum *et al.*[211] This method requires in-air profile penumbra (80%–20%) for different isocenter-to-detector distance for the largest cone that can be measured with films[217] or a diode.[34]

V.B.4. Specific data for Monte Carlo based dose calculation

Many studies have been carried out on the commissioning of electron beams using Monte Carlo simulation.[13,157,210,218–221] These studies have demonstrated the potential of Monte Carlo techniques for generating beam data normally obtained by measurement during the commissioning. The data including the phase space data (i.e., the charge, position, direction, energy, and history tag for each particle), may be required for Monte Carlo based treatment planning. Monte Carlo simulations need to be combined with measurements to validate the Monte Carlo calculations. In addition to those conventional measured data (e.g., PDD, profiles, output factors, absolute dose), there may be other commissioning information required for a Monte Carlo based system.[9,13,220–226] During electron beam commissioning, data for validating Monte Carlo generated energy spectrum and dose calculation can be acquired. Different Monte Carlo algorithm, such as voxel Monte Carlo[222] or macro Monte Carlo,[223,224] may require a different set of data specific for commissioning.

VI. PROCESSING BEAM DATA

VI.A. Processing and manipulations

Following collection of both scan and nonscan beam data, it may be necessary to do some processing before entering the data into a TPS. For scan data, most scanning systems have numerous tools to process beam data, such as smoothing, centering of the beam, and making the beam symmetrical. The amount of processing depends on the type of scanner (e.g., scanning with diodes or in continuous dose rate mode), the accuracy of setup, and characteristics of the machine itself.

VI.B. Smoothing, mirroring, and summarizing

All measured data have a varying degree of noise depending on the system. Smoothing and filtering routines help remove noise and extract actual data. This is also a low pass filtering, i.e., it eliminates high frequencies (abrupt, sharp, spike, and wiggle). Numerous smoothing routines exist, i.e., least square, median, arithmetic mean, geometric mean, moving average, cubic spline, exponential, envelope, Gaussian, Fourier transform, and Beziér.[227–229] However, not all routines will give acceptable results. Typically, one must experiment with different smoothing routines available to see which routine produces the desired results without compromising the basic shape of the scan curve, i.e., eliminate the noise in the scan without changing the basic shape, such as clipping the peak in dose profile of 60° wedge. If the degree of smoothing required is excessive, consideration should be given to repeating the scan using slower scan speeds and/or increased sampling time to improve the data acquisition. The centering tool on most scanning systems works well with open fields. However, if the amount of recentering is excessive (e.g., >0.05 cm), consideration should be given to improving the scanning setup to achieve better centering on the beam since the centering tool will not work on the wedged fields, thereby introducing an error in the position. Most scanning software has a "make symmetrical" or "mirror" tool which works well with open fields. However, if the amount of asymmetry being removed is excessive (e.g., $>0.5\%$ asymmetry) in an open field scan, either the scanning setup should be checked for level or the machine adjusted to improve symmetry as there is no method to remove open field asymmetry from a wedged field. With all these tools, if significant processing, i.e., centering, smoothing, mirroring to correct for asymmetry, is required, it is recommended that consideration be given to recollecting beam data as a good data set should require minimal processing.

VI.B.1. Mathematical functions and filters

Most scanning systems provide a complete description of the functions and filters used for smoothing, mirroring, and summarizing. Refer to the manufacturer's description for information relevant to your system. In general, moving average, cubic-spline, interpolation, and Fourier transform type of functions are available on scanning software. The user should use caution and check the validity of these functions by comparing published reference field data.

VI.B.2. Distortion in smoothing

Most scanning systems have various filters to smooth data. The most common one is the cubic-spline method. Smoothing original data often distorts the data, which are pronounced in the high gradient region, such as penumbra and in wedge profiles. Figure 13 shows the impact of smoothing with an iterative approach. There is no rule or published information as to how much smoothing should be allowed. However, the user should use common sense not to distort the data but simply to smooth it. One to two passes of smoothing should be acceptable. It is always a good practice to keep the original data intact for future evaluation.

VI.C. Processing nonscanned data

For nonscan data, it is recommended that all the beam parameters be plotted to highlight obvious errors (i.e., outliers on curve) to improve the accuracy of data entered into TPS. For example, the plot of output factors (S_c,S_p) versus field size should exhibit a smooth curve with slope that is steep for small fields and relatively flat for large fields.

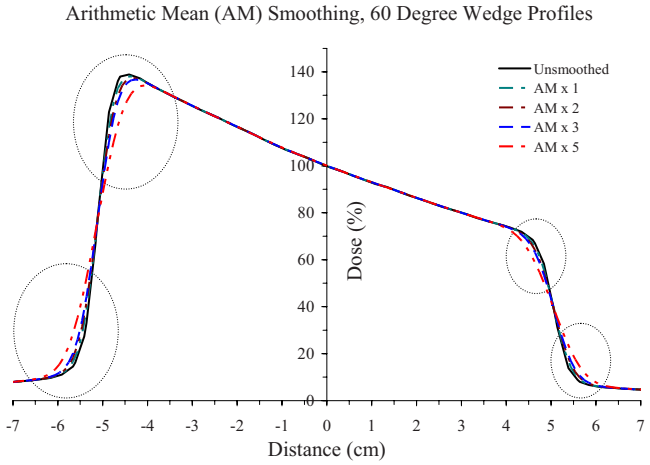

FIG. 13. Effect of data smoothing on the 6 MV 60° wedge profiles. Circles are drawn to show the effect of smoothing.

Points, which obviously do not fit the curve, should be rechecked for computational errors or remeasured, if necessary, to improve the accuracy of the data.

VII. SUMMARY AND RECOMMENDATION

VII.A. Recommendations

As with any report, this document reflects the state of the art at the time of writing, but will age as developments take place in the machine, planning, and measurement technologies. Some of these developments may conflict with recommendations in this report, so the reader should always review recent developments and use this report as a general guide.

(1) Define the scope of data collection based on type of machine, requirements specific to the TPS, operational difficulties, machine's operational condition, and beam energies.
(2) Roughly, calculate the time needed to commission the machine based on assumption as noted in Eq. (1).
(3) Use a proper detector that has high sensitivity, small dimensions, low noise, and minimum dose rate and energy dependence.
(4) Ion chambers with small volumes are generally preferred for relative dosimetry in a photon beam.
(5) Diodes are preferred detectors for relative dosimetry in an electron beam except the bremsstrahlung portion where an electron diode may have a different photon response. For accurate measurement of a bremsstrahlung component, an ion chamber should be used.
(6) Verify the labeling and positional accuracy of the scanning system before starting measurements.
(7) Set optimal speed, time delay, and acquisition time for the scanning system.
(8) Scan from the deepest depth to the surface rather than surface to depth when scanning for PDD.
(9) Adjust the step size for data collection appropriately to optimize the time needed for the collection and accuracy of data.
(10) Maintain proper bias and polarity of detectors, if required.
(11) Minimize the amount of cable in the beam.
(12) Orient the detector mount so that it provides the highest resolution.
(13) Use normalization points and procedures that are as close as possible to the reference conditions for TPS; for photon beams pay particular attention to avoid errors from electron contamination at superficial depths, i.e., avoid d_{max} normalizations.
(14) Write a concise report with all the collected data.
(15) Check on the report and collected data. Have a qualified medical physicist perform an independent audit of the collected data and subsequent report.
(16) Backup entire electronic data, analyzed data, and spread sheets.
(17) Vendor provided data could be used as a reference but it should never be used as a substitute for the commissioned data.

VII.B. Precautions

(1) Do not rely on the manufacturer supplied beam data. Always verify the accuracy since beam data can vary from machine to machine of the same model from the same vendor.
(2) Do not use acceptance testing data for commissioning data, as these are for reference purposes only and are often taken under limited scatter condition.
(3) Do not scan in the axial direction of the detector.
(4) Do not overprocess the data by smoothing or the use of mathematical filters.
(5) Pay attention to the data collected. Any anomaly should be investigated and understood immediately before proceeding to further scanning.
(6) Check the water phantom level at least once a day.

VII.C. Commissioning report

It is recommended that a clear and descriptive report of the commissioning data with proper signature and date be written so that this data can be verified in the future and in case of litigation, some degree of accountability can be maintained. The following is a sample of what should be included in the report.

(1) Formal commissioning report, which clearly outlines the scope of the project, what was measured, how, what equipment was used, and the results, with appropriate attention to describing normalization procedures
(2) Open field x-ray PDD and TMR tables
(3) Wedged field x-ray PDD and TMR tables
(4) X-ray output factor tables (S_{cp},S_c,S_p)
(5) Field size and depth dependent wedge factor tables
(6) Soft wedge (electronic wedge) factor tables
(7) Transmission factor tables
(8) Open field off axis tables at selected depths, large field sizes

(9) Wedge field off axis tables at selected depths, largest field size for wedge
(10) Soft wedge off axis tables at selected depths, largest field size for wedge
(11) Electron cone ratios and effective source distances
(12) Electron PDD tables
(13) Provide at least selected isodose curves for reference fields both for electron and photon beams from PDD and profiles.
(14) Printout of all scan data
(15) Compare data from similar machines within your own department or from different institutions. Comparison to vendor supplied golden data is also acceptable but do not blindly use this data.
(16) Vendor provided data could be used as a reference but it should never be used as a substitute for the commissioned data.
(17) Backup entire electronic data, analyzed data and spread sheets.
(18) Write the report with detailed description of how the beam data were collected and conditions of the beam data collection.

ACKNOWLEDGMENTS

Support from James Pinkerton of Sun Nuclear in editing and organizing this report is greatly appreciated. The authors also thank Ying Xiao, David Followill, Per Halvorsen, Douglas Frye, and other members of the TPC for critical review of the report.

[a]Present address: Indiana University School of Medicine, Indianapolis, IN 46202-5289. Electronic mail: idas@iupui.edu

[1]TG-40, "Comprehensive QA for radiation oncology: Report of AAPM Radiation Therapy Committee Task Group 40," Med. Phys. **21**, 581–618 (1994).
[2]TG-53, "American Association of Physicists in Medicine Radiation Therapy Committee Task Group 53: Quality assurance for clinical radiotherapy treatment planning," Med. Phys. **25**, 1773–1829 (1998).
[3]P. D. LaRiviere, "The quality of high-energy x-ray beams," Br. J. Radiol. **62**, 473–481 (1989).
[4]A. Kosunen and D. W. O. Rogers, "Beam quality specification fro photon beam dosimetry," Med. Phys. **20**, 1181–1188 (1993).
[5]N. I. Kalach and D. W. O. Rogers, "Which accelerator photon beams are clinic-like for reference dosimetry purposes?," Med. Phys. **30**, 1546–1555 (2003).
[6]D. S. Followill, R. C. Tailor, V. M. Tello, and W. F. Hanson, "An empirical relationship for determining photon beam quality in TG-21 from a ratio of percent depth doses," Med. Phys. **25**, 1202–1205 (1998).
[7]R. C. Tailor, V. M. Tello, C. B. Schroy, M. Vossler, and W. F. Hanson, "A generic off-axis energy correction for linac photon beam dosimetry," Med. Phys. **25**, 662–667 (1998).
[8]R. C. Tailor, D. S. Followill, and W. F. Hanson, "A first order approximation of field-size and depth dependence of wedge transmission," Med. Phys. **25**, 241–244 (1998).
[9]A. Tzedakis, J. Damilakis, M. Mazonakis, J. Stratakis, H. Varveris, and N. Gourtsoyiannis, "Influence of initial electron beam parameters on Monte Carlo calculated absorbed dose distributions for radiotherapy photon beams," Med. Phys. **31**, 907–913 (2004).
[10]G. X. Ding, "An investigation of accelerator head scatter and output factor in air," Med. Phys. **31**, 2527–2533 (2004).
[11]G. X. Ding, "Using Monte Carlo simulations to commission photon beam output factors-a feasibility study," Phys. Med. Biol. **48**, 3865–3874 (2003).
[12]P. J. Keall, J. V. Siebers, R. Jeraj, and R. Mohan, "The effect of dose calculation uncertainty on the evaluation of radiotherapy plans," Med. Phys. **27**, 478–484 (2000).
[13]G. X. Ding, D. M. Duggan, and C. W. Coffey, "Commissioning stereotactic radiosurgery beams using both experimental and theoretical methods," Phys. Med. Biol. **51**, 2549–2566 (2006).
[14]TG-10, "Code of practice for x-ray therapy linear accelerators," Med. Phys. **2**, 110–121 (1975).
[15]R. Nath, P. J. Biggs, F. J. Bova, C. C. Ling, J. A. Purdy, J. Van de Geijn, and M. S. Weinhous, "AAPM code of practice for radiotherapy accelerators: Report of AAPM Radiation Therapy Task Group No. 45," Med. Phys. **21**, 1093–1121 (1994).
[16]IPEM Report No. 94, "Acceptance testing and commissioning of linear accelerators," Institute of Physics and Engineering in Medicine, 2007.
[17]AAPM Report No. 54, *Stereotactic Radiosurgery: Report of the Task Group 42, Radiation Therapy Committee*, AAPM Report No. 54 (American Institute of Physics, Woodbury, NY, 1995).
[18]G. Ezzell, J. Galvin, D. Low, J. R. Palta, I. Rosen, M. B. Sharpe, P. Xia, Y. Xiao, L. Xing, and C. Yu, "Guidance document on delivery, treatment planning, and clinical implementation of IMRT: Report of the IMRT Subcommittee of the AAPM Radiation Therapy Committee," Med. Phys. **30**, 2089–2115 (2003).
[19]TG-120, "Working group on IMRT metrology," (unpublished).
[20]TG-74, "In-air output ratio, S_c, for megavoltage photon beams. Report of the AAPM Radiation Therapy Committee Task Group No. 74," (unpublished).
[21]S. Pai, I. J. Das, J. F. Dempsey, K. L. Lam, T. J. LoSasso, A. J. Olch, J. R. Palta, L. E. Reinstein, D. Ritt, and E. E. Wilcox, "TG-69: Radiographic film for megavoltage beam dosimetry," Med. Phys. **34**, 2228–2258 (2007).
[22]TG-70, "Recommendations for clinical electron beam dosimetry: supplement to the recommendations of Task Group 25," (unpublished).
[23]AAPM Report No. 23, *Total Skin Electron Therapy: Technique and Dosimetry*, AAPM Report No. 23, (American Institute of Physics, Woodbury, NY, 1988).
[24]AAPM Report No. 17, "The physical aspects of total and half body photon irradiation," American Association of Physicists in Medicine, 1986.
[25]M. G. Marshall, "Matching the 6-MV photon beam characteristics of two dissimilar linear accelerators," Med. Phys. **20**, 1743–1746 (1992).
[26]J. Hrbacek, T. Depuydt, A. Nulens, A. Swinnen, and F. Van den Heuvel, "Quantitative evaluation of a beam-matching procedure using one-dimensional gamma analysis," Med. Phys. **34**, 2917–2927 (2007).
[27]I. J. Das and T. C. Zhu, "Thermal and temporal response of ionization chambers in radiation dosimetry," Med. Phys. **31**, 573–578 (2004).
[28]A. Ho and B. R. Paliwal, "Stopping-power and mass energy-absorption coefficient ratios for solid water," Med. Phys. **13**, 403–404 (1986).
[29]V. M. Tello, R. C. Tailor, and W. F. Hanson, "How water equivalent are water-equivalent solid materials for output calibration of photon and electron beams?," Med. Phys. **22**, 1177–1189 (1995).
[30]R. C. Tailor, C. Chu, D. S. Followill, and W. F. Hanson, "Equilibration of air temperature inside the thimble of a Farmer-type ion chamber," Med. Phys. **25**, 496–502 (1998).
[31]L. Weber, P. Nilsson, and A. Ahnesjö, "Build-up cap materials for measurement of photon head-scatter factors," Phys. Med. Biol. **42**, 1875–1886 (1997).
[32]J. Li and T. C. Zhu, "Measurement of in-air output ratios using different miniphantom materials," Phys. Med. Biol. **51**, 3819–3834 (2006).
[33]L. J. Humphries and J. A. Purdy, in *Advances in Radiation Oncology Physics Dosimetry, Treatment Planning, and Brachytherapy: Medical Physics Monograph No. 19*, edited by J. A. Purdy (American Institute of Physics, New York, 1992), pp. 111–147.
[34]G. Rickner, "Silicon diodes as detectors in relative dosimetry of photon, electron and proton radiation fields," Uppsala Universsitet, 1983.
[35]G. Rickner and E. Grusell, "Effect of radiation damage on *p*-type silicon detectors," Phys. Med. Biol. **28**, 1261–1267 (1983).
[36]G. Rickner and E. Grusell, "General specifications for silicon semiconductors for use in radiation dosimetry," Phys. Med. Biol. **32**, 1109–1117 (1987).
[37]A. S. Saini and T. C. Zhu, "Temperature dependence of commercially available diode detectors," Med. Phys. **29**, 622–630 (2002).
[38]A. S. Saini and T. C. Zhu, "Dose rate and SDD dependence of commercially available diode detectors," Med. Phys. **31**, 914–924 (2004).
[39]TG-62, *Diode in vivo dosimetry for patients receiving external beam radiation therapy, Report of the AAPM radiation therapy committee Task Group No. 62* (Medical Physics, Madison, WI, 2005).

[40]I. Griessbach, M. Lapp, J. Bohsung, G. Gademann, and D. Harder, "Dosimetric characteristics of a new unshielded silicon diode and its application in clinical photon and electron beams," Med. Phys. **32**, 3750–3754 (2005).
[41]J. Shi, W. E. Simon, and T. C. Zhu, "Modeling the instantaneous dose rate dependence of radiation diode detectors," Med. Phys. **30**, 2509–2519 (2003).
[42]H. Song, M. Ahmad, J. Deng, Z. Chen, N. J. Yue, and R. Nath, "Limitations of silicon diodes for clinical electron dosimetry," Radiat. Prot. Dosim. **120**, 56–59 (2006).
[43]L. L. Wang and D. W. Rogers, "Monte Carlo study of Si diode response in electron beams," Med. Phys. **34**, 1734–1742 (2007).
[44]N. P. Sidhu, "Interfacing a linear diode array to a conventional water scanner for the measurement of dynamic dose distributions and comparison with a linear ion chamber array," Med. Dosim. **24**, 57–60 (1999).
[45]T. C. Zhu, L. Ding, C. R. Liu, J. R. Palta, W. E. Simon, and J. Shi, "Performance evaluation of a diode array for enhanced dynamic wedge dosimetry," Med. Phys. **24**, 1173–1180 (1997).
[46]M. Heydarian, P. W. Hoban, W. A. Beckham, I. A. Borchardt, and A. H. Beddoe, "Evaluation of a PTW diamond detector for electron beam measurements," Phys. Med. Biol. **38**, 1035–1042 (1993).
[47]P. W. Hoban, M. Heydarian, W. A. Beckham, and A. H. Beddoe, "Dose rate dependence of a PTW diamond detector in the dosimetry of a 6 MV photon beam," Phys. Med. Biol. **39**, 1219–1229 (1994).
[48]V. S. Khrunov, S. S. Martynov, S. M. Vatnisky, I. A. Ermakov, A. M. Chervjakov, D. L. Karlin, V. I. Fominych, and Y. V. Tarbeyev, "Diamond detectors in relative dosimetry of photon, electron and proton radiation fields," Radiat. Prot. Dosim. **33**, 155–157 (1990).
[49]W. U. Laub, T. W. Kaulich, and F. Nusslin, "Energy and dose rate dependence of a diamond detector in the dosimetry of 4–25 MV photon beams," Med. Phys. **24**, 535–536 (1997).
[50]S. Vatnitsky and H. Järvinen, "Application of natural diamond detector for the measurement of relative dose distributions in radiotherapy," Phys. Med. Biol. **38**, 173–184 (1993).
[51]Y. S. Horowitz, "The theoretical and microdosimetric basis of thermoluminescence and applications to dosimetry," Phys. Med. Biol. **26**, 765–824 (1981).
[52]P. N. Mobit, P. Mayles, and A. E. Nahum, "The quality dependence of LiF TLD in megavoltage photon beams: Monte Carlo simulation and experiments," Phys. Med. Biol. **41**, 387–398 (1996).
[53]P. N. Mobit, A. E. Nahum, and P. Mayles, "The energy correction factor of LiF thermoluminescent dosemeters in megavoltage electron beams: Monte Carlo simulations and experiments," Phys. Med. Biol. **41**, 979–993 (1996).
[54]L. Duggan, C. Hood, H. Warren-Forward, M. Haque, and T. Kron, "Variations in dose response with x-ray energy of LiF:Mg, Cu, P thermoluminescence dosimeters: Implications for clinical dosimetry," Phys. Med. Biol. **49**, 3831–3845 (2004).
[55]A. Niroomand-Rad, C. R. Blackwell, B. M. Coursey, K. P. Gall, J. M. Galvin, W. L. McLaughlin, A. S. Meigooni, R. Nath, J. E. Rodgers, and C. G. Soares, "Radiographic film dosimetry: Recommendations of AAPM Radiation Therapy Committee Task Group 55," Med. Phys. **25**, 2093–2115 (1998).
[56]TG-25, "Clinical electron beam dosimetry: Report of AAPM Radiation Therapy Committee Task Group No. 25," Med. Phys. **18**, 73–109 (1991).
[57]R. Ramani, A. W. Lightstone, D. L. Mason, and P. F. O'Brien, "The use of radiochromic film in treatment verification of dynamic stereotactic radiosurgery," Med. Phys. **21**, 389–392 (1994).
[58]J. L. Robar and B. G. Clark, "The use of radiographic film for linear accelerator stereotactic radiosurgical dosimetry," Med. Phys. **26**, 2144–2150 (1999).
[59]D. D. Leavitt and E. Klein, "Dosimetry measurement tools for commissioning enhanced dynamic wedge," Med. Dosim. **22**, 171–176 (1997).
[60]F. F. Yin, "Physical penumbra change of beam profile due to film digitization," Med. Phys. **22**, 803–805 (1995).
[61]R. Ramani, S. Russell, and P. F. O'Brien, "Clinical dosimetry using MOSFETs," Int. J. Radiat. Oncol., Biol., Phys. **37**, 959–964 (1997).
[62]C. F. Chuang, L. Verhey, and P. Xia, "Investigation of the use of MOSFET for clinical IMRT dosimetric verification," Med. Phys. **29**, 1109–1115 (2002).
[63]G. S. Ibbott, M. J. Maryanski, P. Eastman, S. D. Holcomb, Y. Zhang, R. G. Avison, M. Sanders, and J. C. Gore, "Three-dimensional visualization and measurement of conformal dose distributions using magnetic resonance imaging of BANG polymer gel dosimeters," Int. J. Radiat. Oncol., Biol., Phys. **38**, 1097–1103 (1997).
[64]R. K. Rice, J. L. Hansen, G. K. Svensson, and R. L. Siddon, "Measurements of dose distributions in small beams of 6 MV x-rays," Phys. Med. Biol. **32**, 1087–1099 (1987).
[65]P. Francescon, S. Cora, and P. Chiovati, "Dose verification of an IMRT treatment planning system with BEAM, EGS-based Monte Carlo code," Med. Phys. **30**, 144–157 (2003).
[66]W. U. Laub and T. Wong, "The volume effect of detectors in the dosimetry of small fields used in IMRT," Med. Phys. **30**, 341–347 (2003).
[67]F. Sanchez-Doblado, R. Capote, A. Leal, J. V. Rosello, J. I. Lagares, R. Arrans, and G. H. Hartmann, "Micro ionization chamber for reference dosimetry in IMRT verification: Clinical implications on OAR dosimetric errors," Phys. Med. Biol. **50**, 959–970 (2005).
[68]F. Araki, "Monte Carlo study of a Cyberknife stereotactic radiosurgery system," Med. Phys. **33**, 2955–2963 (2006).
[69]G. Bednarz, S. Huq, and U. F. Rosenow, "Deconvolution of detector size effect for output factor measurement for narrow Gamma Knife radiosurgery beams," Phys. Med. Biol. **47**, 3643–3649 (2002).
[70]P. D. Higgins, C. H. Sibata, L. Siskind, and J. W. Sohn, "Deconvolution of detector size effect for small field measurement," Med. Phys. **22**, 1663–1666 (1995).
[71]F. Garcia-Vicente, J. M. Delgado, and C. Peraza, "Experimental determination of the convolution kernel for the study of the spatial response of a detector," Med. Phys. **25**, 202–207 (1998).
[72]P. Charland, E. el-Khatib, and J. Wolters, "The use of deconvolution and total least squares in recovering a radiation detector line spread function," Med. Phys. **25**, 152–160 (1998).
[73]D. Herrup, J. Chu, H. Cheung, and M. Pankuch, "Determination of penumbral widths from ion chamber measurements," Med. Phys. **32**, 3636–3640 (2005).
[74]K. S. Chang, F. F. Yin, and K. W. Nie, "The effect of detector size to the broadening of the penumbra—A computer simulated study," Med. Phys. **23**, 1407–1411 (1996).
[75]C. H. Sibata, H. C. Mota, A. S. Beddar, P. D. Higgins, and K. H. Shin, "Influence of detector size in photon beam profile measurements," Phys. Med. Biol. **36**, 621–631 (1991).
[76]D. J. Dawson, J. M. Harper, and A. C. Akinradewo, "Analysis of physical parameters associated with the measurement of high-energy x-ray penumbra," Med. Phys. **11**, 491–497 (1984).
[77]P. Metcalfe, T. Kron, A. Elliott, T. Wong, and P. Hoban, "Dosimetry of 6-MV x-ray beam penumbra," Med. Phys. **20**, 1439–1445 (1993).
[78]T. Kron, A. Elliott, and P. Metcalfe, "The penumbra of a 6-MV x-ray beam as measured by thermoluminescent dosimetry and evaluated using an inverse square root function," Med. Phys. **20**, 1429–1438 (1993).
[79]D. E. Mellenberg, R. A. Dahl, and C. R. Blackwell, "Acceptance testing of an automated scanning water phantom," Med. Phys. **17**, 311–314 (1990).
[80]M. G. Schmid and R. L. Morris, "A water phantom controller for automated acquisition of linac beam parameters," Med. Phys. **16**, 126–129 (1989).
[81]Y. K. Kim, S. H. Park, H. S. Kim, S. M. Kang, J. H. Ha, C. E. Chung, S. Y. Cho, and J. K. Kim, "Polarity effect of the thimble-type ionization chamber at a low dose rate," Phys. Med. Biol. **50**, 4995–5003 (2005).
[82]TG-51, "AAPM's TG-51 protocol for clinical reference dosimetry of high-energy photon and electron beams," Med. Phys. **26**, 1847–1870 (1999).
[83]B. Gross, "The Compton current," Z. Phys. **155**, 479–487 (1959).
[84]J. F. Fowler and F. T. Farmer, "Conductivity induced in insulating materials by x-rays," Nature (London) **173**, 317–318 (1954).
[85]J. J. Spokas and R. D. Meeker, "Investigation of cables for ionization chambers," Med. Phys. **7**, 135–140 (1980).
[86]I. J. Das, J. F. Copeland, and H. S. Bushe, "Spatial distribution of bremsstrahlung in a dual electron beam used in total skin electron treatments: Errors due to ionization chamber cable irradiation," Med. Phys. **21**, 1733–1738 (1994).
[87]I. J. Das, S. W. McNeeley, and C.-W. Cheng, "Ionization chamber shift correction and surface dose measurements in electron beams," Phys. Med. Biol. **43**, 3419–3424 (1998).
[88]F. M. Khan, *The Physics of Radiation Therapy*, 3rd ed. (Lippincott Williams & Wilkins, Philadelphia, PA, 2003).
[89]G. S. Ibbott, J. E. Barne, G. R. Hall, and W. R. Hendee, "Stem corrections for ionization chambers," Med. Phys. **2**, 328–330 (1975).

[90]B. J. Gerbi and F. M. Khan, "Measurement of dose in the buildup region using fixed-separation plane-parallel ion chambers," Med. Phys. **17**, 17–26 (1990).
[91]R. L. Stern and H. D. Kubo, "Considerations for superficial photon dosimetry," Med. Phys. **22**, 1469–1470 (1995).
[92]B. Nilsson and A. Brahme, "Electron contamination from photon beam collimators," Radiother. Oncol. **5**, 235–244 (1986).
[93]R. Sjögren and M. Karlsson, "Electron contamination in clinical high energy photon beams," Med. Phys. **23**, 1873–1881 (1996).
[94]B. Nilsson, "Electron contamination from different materials in high energy photon beams," Phys. Med. Biol. **30**, 139–151 (1985).
[95]F. M. Khan, V. C. Moore, and S. H. Levitt, "Effect of various atomic number absorbers on skin dose for 10-MeV x rays," Radiology **109**, 209–212 (1973).
[96]P. J. Biggs and M. D. Russell, "An investigation into the presence of secondary electrons in megavoltage photon beams," Phys. Med. Biol. **28**, 1033–1043 (1983).
[97]T. C. Zhu and J. R. Palta, "Electron contamination in 8 and 18 MV photon beams," Med. Phys. **25**, 12–19 (1998).
[98]P. J. Biggs and C. C. Ling, "Electrons as the cause of the observed dmax shift with field size in high energy photon beams," Med. Phys. **6**, 291–295 (1979).
[99]E. D. Yorke, C. C. Ling, and S. Rustgi, "Air-generated electron contamination of 4 and 10 MV photon beams: A comparison of theory and experiment," Phys. Med. Biol. **30**, 1305–1314 (1985).
[100]B. E. Bjärngard, P. Vadash, and T. Zhu, "Doses near the surface in high-energy x-ray beams," Med. Phys. **22**, 465–468 (1995).
[101]A. Lopez Medina, A. Teijeiro, J. Garcia, J. Esperon, J. A. Terron, D. P. Ruiz, and M. C. Carrion, "Characterization of electron contamination in megavoltage photon beams," Med. Phys. **32**, 1281–1292 (2005).
[102]E. E. El-Khatib, J. Scrimger, and B. Murray, "Reduction of the bremsstrahlung component of clinical electron beams: implications for electron arc therapy and total skin electron irradiation," Phys. Med. Biol. **36**, 111–118 (1991).
[103]H. Svensson, "Influence of scattering foils, transmission monitors and collimating system on the absorbed dose distribution from 10–35 MeV electron irradiation," Acta Radiol. Ther. Phys. Biol. **10**, 443–453 (1971).
[104]BJR Supply 25, "Central axis depth dose data for use in radiotherapy: 1996," Br. J. Radiol. Supplement 25, British Institute of Radiology, 1996.
[105]N. Dogan and G. Glasgow, "Surface and build-up region dosimetry for obliquely incident intensity modulated radiotherapy 6 MV x rays," Med. Phys. **30**, 3091–3096 (2003).
[106]A. R. Hounsell and J. M. Wilkinson, "Electron contamination and build-up doses in conformal radiotherapy fields," Phys. Med. Biol. **44**, 43–55 (1999).
[107]A. Lamb and S. Blake, "Investigation and modeling of the surface dose from linear accelerator produced 6 and 10 MV photon beams," Phys. Med. Biol. **43**, 1133–1146 (1998).
[108]M. G. McKenna, X. G. Chen, M. D. Altschuler, and P. Block, "Calculation of the dose in the build-up region for high energy photon beam. Treatment planning when beam spoilers are employed," Radiother. Oncol. **34**, 63–68 (1995).
[109]D. P. Fontenla, J. J. Napoli, M. Hunt, D. Fass, B. McCormick, and G. J. Kutcher, "Effects of beam modifiers and immobilization devices on the dose in the build-up region," Int. J. Radiat. Oncol., Biol., Phys. **30**, 211–219 #x0028;1994).
[110]E. C. McCullough, "A measurement and analysis of buildup region dose for open field photon beams (Co-60 through 24 MV)," Med. Dosim. **19**, 5–14 (1994).
[111]F. Habibollahi, H. M. O. Mayles, P. J. Winter, D. Tong, I. S. Fentiman, M. A. Chaudary, and J. L. Hayward, "Assessment of skin dose and its relation to cosmesis in the conservative treatment of early breast cancer," Int. J. Radiat. Oncol., Biol., Phys. **14**, 291–296 (1988).
[112]D. E. Velkley, D. J. Manson, J. A. Purdy, and G. D. Oliver, "Buildup region of megavoltage photon radiation sources," Med. Phys. **2**, 14–19 (1975).
[113]E. E. Klein, J. Esthappan, and Z. Li, "Surface and buildup dose characteristics for 6, 10, and 18 MV photons from an Elekta Precise linear accelerator," J. Appl. Clin. Med. Phys. **4**, 1–7 (2003).
[114]K. Y. Quach, J. Morales, M. J. Butson, A. B. Rosenfeld, and P. E. Metcalfe, "Measurement of radiotherapy x-ray skin dose on a chest wall phantom," Med. Phys. **27**, 1676–1680 (2000).
[115]S. Kim, C. R. Liu, T. C. Zhu, and J. R. Palta, "Photon beam skin dose analyses for different clinical setups," Med. Phys. **25**, 860–866 (1998).
[116]D. J. Manson, D. Velkley, J. A. Purdy, and G. D. Oliver, "Measurements of surface dose using build-up curves obtained with an extrapolation chamber," Radiology **115**, 473–474 (1975).
[117]S. Heukelom, J. H. Lanson, and B. J. Mijnheer, "Comparison of entrance and exit dose measurements using ionization chambers and silicon diodes," Phys. Med. Biol. **36**, 47–59 (1991).
[118]D. Georg, B. De Ost, M. T. Hoornaert, P. Pilette, J. Van Dam, M. Van Dyke, and D. Huyskens, "Build-up modification of commercial diodes for entrance dose measurements in 'higher energy' photon beams," Radiother. Oncol. **51**, 249–256 (1999).
[119]D. E. Mellenberg, "Determination of buildup-up region over-response corrections for a Markus-type chamber," Med. Phys. **17**, 1041–1044 (1990).
[120]M. Butson, A. Rozenfeld, J. N. Mathur, M. Carolan, T. P. Y. Wong, and P. E. Metcalfe, "A new radiotherapy surface dose detector: The MOSFET," Med. Phys. **23**, 655–658 (1996).
[121]M. J. Butson, J. N. Mathur, and P. E. Metcalfe, "Radiochromic film as a radiotherapy surface-dose detector," Phys. Med. Biol. **41**, 1073–1078 (1996).
[122]A. Ahnesjö, L. Weber, A. Murman, M. Saxner, I. Thorslund, and E. Traneus, "Beam modeling and verification of a photon beam multisource model," Med. Phys. **32**, 1722–1737 (2005).
[123]P. Keall, S. Zavgorodni, L. Schidt, and D. Haskard, "Improving wedged field dose distributions," Phys. Med. Biol. **42**, 2183–2192 (1997).
[124]U. Myler and J. J. Szabo, "Dose calculation along the nonwedged direction," Med. Phys. **29**, 746–754 (2002).
[125]I. J. Das, G. E. Desobry, S. W. McNeeley, E. C. Cheng, and T. S. Schultheiss, "Beam characteristics of a retrofitted double-focused multileaf collimator," Med. Phys. **25**, 1676–1684 (1998).
[126]J. M. Galvin, K. Han, and R. Cohen, "A comparison of multileaf collimator and alloy-block field shaping," Int. J. Radiat. Oncol., Biol., Phys. **40**, 721–731 (1998).
[127]P. Xia, P. Geis, L. Xing, C. Ma, D. Findley, K. Forster, and A. Boyer, "Physical characteristics of a miniature multileaf collimator," Med. Phys. **26**, 65–70 (1999).
[128]J. R. Sykes and P. C. Williams, "An experimental investigation of the tongue and groove effect for the Philips multileaf collimator," Phys. Med. Biol. **43**, 3157–3165 (1998).
[129]S. Webb, T. Bortfeld, J. Stein, and D. Convery, "The effect of stair-step leaf transmission on the 'tongue-and-groove problem' in dynamic radiotherapy with a multileaf collimator," Phys. Med. Biol. **42**, 595–602 (1997).
[130]A. S. Shiu, H. M. Kooy, J. R. Ewton, S. S. Tung, J. Wong, K. Antes, and M. H. Maor, "Comparison of miniature multileaf collimation (MMLCC) with circular collimation for stereotactic treatment," Int. J. Radiat. Oncol., Biol., Phys. **37**, 679–688 (1997).
[131]D. A. Low, J. W. Sohn, E. E. Klein, J. Markman, S. Mutic, and J. F. Dempsey, "Characterization of a commercial multileaf collimator used for intensity modulated radiation therapy," Med. Phys. **28**, 752–756 (2001).
[132]AAPM Report No. 72, *Basic Applications of Multileaf Collimators: Report of the AAPM Radiation Therapy Committee Task Group No. 50*, AAPM Report No. 50 (American Institute of Physics by Medical Physics Publishing, Madison, WI, 2001).
[133]T. LoSasso, C. Chui, and C. Ling, "Comprehensive quality assurance for the delivery of intensity modulated radiotherapy with a multileaf collimator used in the dynamic mode," Med. Phys. **28**, 2209–2219 (2001).
[134]M. Woo, P. Charland, B. Kim, and A. Nico, "Commissioning, evaluation, quality assurance and clinical application of a virtual micro MLC technique," Med. Phys. **30**, 138–143 (2003).
[135]J. E. Bayouth and S. M. Morrill, "MLC dosimetric characteristics for small field and IMRT applications," Med. Phys. **30**, 2545–2552 (2003).
[136]J. M. Galvin, A. R. Smith, and B. Lilly, "Characterization of a multi-leaf collimator system," Int. J. Radiat. Oncol., Biol., Phys. **25**, 181–192 (1993).
[137]T. J. Jordan and P. C. Williams, "The design and performance characteristics of a multileaf collimator," Phys. Med. Biol. **39**, 231–251 (1994).
[138]M. S. Huq, I. J. Das, T. Steinberg, and J. M. Galvin, "A dosimetric comparison of various multileaf collimators," Phys. Med. Biol. **47**, N159–N170 (2002).
[139]G. H. Hartmann and F. Fohlisch, "Dosimetric characterization of a new miniature multileaf collimator," Phys. Med. Biol. **47**, N171–N177 (2002).

[140]F. Crop, N. Reynaert, G. Pittomvils, L. Paelinck, W. De Gersem, C. De Wagter, L. Vakaet, W. De Neve, and H. Thierens, "Monte Carlo modeling of the ModuLeaf miniature MLC for small field dosimetry and quality assurance of the clinical treatment planning system," Phys. Med. Biol. **52**, 3275–3290 (2007).
[141]A. L. Boyer, T. G. Ochran, C. E. Nyerick, T. J. Waldron, and C. J. Huntzinger, "Clinical dosimetry for implementation of a multileaf collimator," Med. Phys. **19**, 1255–1261 (1992).
[142]E. E. Klein, W. B. Harms, D. A. Low, V. Willcut, and J. A. Purdy, "Clinical implementation of a commercial multileaf collimator: Dosimetry, networking, simulation, and quality assurance," Int. J. Radiat. Oncol., Biol., Phys. **33**, 1195–1208 (1995).
[143]V. P. Cosgrove, U. Jahn, M. Pfaender, S. Bauer, V. Budach, and R. E. Wurm, "Commissioning of a micro multileaf collimator and planning system for stereotactic radiosurgery," Radiother. Oncol. **50**, 325–336 (1999).
[144]G. J. Budgell, J. H. Mott, P. C. Williams, and K. J. Brown, "Requirements for leaf position accuracy for dynamic multileaf collimation," Phys. Med. Biol. **45**, 1211–1227 (2000).
[145]TG-50, *American Association of Physicists in Medicine Radiation Therapy Committee Report No. 72. Basic Application of Multileaf Collimators* (Medical Physics Publishing, Madison, WI, 2001).
[146]C. D. Mubata, P. Childs, and A. M. Bidmead, "A quality assurance procedure for the Varian multi-leaf collimator," Phys. Med. Biol. **42**, 423–431 (1997).
[147]M. F. Clarke and G. J. Budgell, "Use of an amorphous silicon EPID for measuring MLC calibration at various gantry angle," Phys. Med. Biol. **53**, 473–485 (2008).
[148]G. Mu, E. Ludlum, and P. Xia, "Impact of MLC leaf position errors on simple and complex IMRT plans for head and neck cancer," Phys. Med. Biol. **53**, 77–88 (2008).
[149]H. V. James, S. Atherton, G. J. Budgell, M. C. Kirby, and P. C. Williams, "Verification of dynamic multileaf collimation using an electronic portal imaging device," Phys. Med. Biol. **45**, 495–509 (2000).
[150]S. M. Huq, Y. Yu, Z.-P. Chen, and N. Suntharalingam, "Dosimetric characteristics of a commercial multileaf collimator," Med. Phys. **22**, 241–247 (1995).
[151]C. W. Cheng, S. H. Cho, M. Taylor, and I. J. Das, "Determination of zero field size percent depth doses and tissue maximum ratios for stereotactic radiosurgery and IMRT dosimetry: Comparison between experimental measurements and Monte Carlo simulation," Med. Phys. **34**, 3149–3157 (2007).
[152]I. J. Das, G. X. Ding, and A. Ahnesjö, "Small fields: Non-equilibrium radiation dosimetry," Med. Phys. **35**, 206–215 (2008).
[153]P. Francescon, S. Cora, and C. Cavedon, "Total scatter factors of small beams: A multidetector and Monte Carlo study," Med. Phys. **35**, 504–513 (2008).
[154]D. W. O. Rogers and A. F. Bielajew, in *The Dosimetry of Ionizing Radiation Volume III*, edited by K. R. Kase, B. E. Bjarngard, and F. H. Attix (Academic, New York, 1990), pp. 427–539.
[155]T. R. Mackie, in *The Dosimetry of Ionizing Radiation Volume III*, edited by K. R. Kase, B. E. Bjarngard, and F. H. Attix (Academic, New York, 1990), pp. 541–562.
[156]P. Andreo, "Monte Carlo techniques in medical radiation physics," Phys. Med. Biol. **36**, 861–920 (1991).
[157]D. W. O. Rogers, B. A. Faddegon, G. X. Ding, C.-M. Ma, and J. We, "BEAM: A Monte Carlo code to simulate radiotherapy treatment units," Med. Phys. **22**, 503–524 (1995).
[158]D. Sheikh-Bagheri and D. W. Rogers, "Monte Carlo calculation of nine megavoltage photon beam spectra using the BEAM code," Med. Phys. **29**, 391–402 (2002).
[159]I. J. Chetty, B. Curran, J. E. Cygler, J. J. DeMarco, G. Ezzell, B. A. Faddegon, I. Kawrakow, P. J. Keall, H. Liu, C. M. Ma, D. W. Rogers, J. Seuntjens, D. Sheikh-Bagheri, and J. V. Siebers, "Report of the AAPM Task Group No. 105: Issues associated with clinical implementation of Monte Carlo-based photon and electron external beam treatment planning," Med. Phys. **34**, 4818–4853 (2007).
[160]K. De Vlamynck, C. De Wagter, and W. De Neve, "Diamond detector measurements near simulated air channels for narrow photon beams," Radiother. Oncol. **53**, 155–159 (1999).
[161]C. M. Ma, M. Ding, J. S. Li, M. C. Lee, T. Pawlicki, and J. Deng, "A comparative dosimetric study on tangential photon beams, intensity-modulated radiation therapy (IMRT) and modulated electron radiotherapy (MERT) for breast cancer treatment," Phys. Med. Biol. **48**, 909–924 (2003).
[162]X. R. Zhu, M. T. Gillin, K. Ehlers, F. Lopez, D. F. Grimm, J. J. Rownd, and T. H. Steinberg, "Dependence of virtual wedge factor on dose calibration and monitor units," Med. Phys. **28**, 174–177 (2001).
[163]F. Verhaegen, I. J. Das, and H. Palmans, "Monte Carlo dosimetry study of 6 MV stereotactic radiosurgery unit," Phys. Med. Biol. **43**, 2755–2768 (1998).
[164]O. A. Sauer and J. Wilbert, "Measurement of output factors for small photon beams," Med. Phys. **34**, 1983–1988 (2007).
[165]S. Kim, J. R. Palta, and T. C. Zhu, "A generalized solution for the calculation of in-air output factors in irregular fields," Med. Phys. **25**, 1692–1701 (1998).
[166]K. R. Kase and G. K. Svensson, "Head scatter data for several linear accelerators (4–18 MV)," Med. Phys. **13**, 530–532 (1986).
[167]M. Tatcher and B. Bjarngard, "Head-scatter factors and effective x-ray source positions in a 25-MV linear accelerator," Med. Phys. **19**, 685–686 (1992).
[168]R. D. Bar-Deroma and B. E. Bjärngard, "The relation between wedge factors in air and water," Med. Phys. **21**, 1043–1047 (1994).
[169]S. Heukelom, J. H. Lanson, and B. J. Mijnheer, "Wedge factor constituents of high energy photon beams: Head and phantom scatter components," Radiother. Oncol. **32**, 73–83 (1994).
[170]E. C. McCullough, J. Gortney, and C. R. Blackwell, "A depth dependence determination of the wedge transmission factor for 4–10 MV photon beams," Med. Phys. **15**, 621–623 (1988).
[171]J. R. Palta, I. Daftari, and N. Suntharlingam, "Field size dependence of wedge factors," Med. Phys. **15**, 624–626 (1988).
[172]R. C. Tailor, D. S. Followill, and W. F. Hanson, "A first order approximation of field size and depth dependence of wedge transmission," Med. Phys. **25**, 241–244 (1998).
[173]S. J. Thomas, "The effect on wedge factors of scattered radiation from the wedge," Radiother. Oncol. **32**, 271–273 (1994).
[174]S. J. Thomas, "The variation of wedge factors with field size on a linear accelerator," Br. J. Radiol. **63**, 355–356 (1990).
[175]C. W. Cheng, W. L. Tang, and I. J. Das, "Beam characteristics of upper and lower physical wedge systems of Varian accelerators," Phys. Med. Biol. **48**, 3667–3683 (2003).
[176]E. E. Klein, R. Gerber, X. R. Zhu, F. Oehmke, and J. A. Purdy, "Multiple machine implementation of enhanced dynamic wedge," Instrum. Control Syst. **40**, 977–985 (1998).
[177]J. P. Gibbons, "Calculation of enhanced dynamic wedge factors for symmetric and asymmetric photon fields," Med. Phys. **25**, 1411–1418 (1998).
[178]G. E. Desobry, T. J. Waldron, and I. J. Das, "Validation of new virtual wedge model," Med. Phys. **25**, 71–72 (1998).
[179]M. J. Zelefsky, T. Hollister, A. Raben, S. Matthews, and K. E. Wallner, "Five-year biochemical outcome and toxicity with transperineal CT-planned permanent I-125 prostate implantation for patients with localized prostate cancer," Int. J. Radiat. Oncol., Biol., Phys. **47**, 1261–1266 (2000).
[180]E. E. Klein, D. A. Low, A. S. Meigooni, and J. A. Purdy, "Dosimetry and clinical implementation of dynamic wedge," Int. J. Radiat. Oncol., Biol., Phys. **31**, 583–592 (1995).
[181]M. H. Phillips, H. Parsaei, and P. S. Cho, "Dynamic and omni wedge implementation on an Elekta SL linac," Med. Phys. **27**, 1623–1634 (2000).
[182]H. Shackford, B. E. Bjarngard, and P. Vadash, "Dynamic universal wedge," Med. Phys. **22**, 1735–1741 (1995).
[183]B. D. Milliken, J. V. Turian, R. J. Hamilton, S. J. Rubin, F. T. Kuchnir, C. X. Yu, and J. W. Wong, "Verification of the omni wedge technique," Med. Phys. **25**, 1419–1423 (1998).
[184]J. Dai, Y. Zhu, and X. Wu, "Verification of the super-omni wedge concept," Phys. Med. Biol. **46**, 2447–2455 (2001).
[185]S. C. Sharma and M. W. Johnson, "Recommendations for measurement of tray and wedge factors for high energy photons," Med. Phys. **21**, 573–575 (1994).
[186]A. E. Nahum, "Perturbation effects in dosimetry: Part I. Kilovoltage x-rays and electrons," Phys. Med. Biol. **41**, 1531–1580 (1996).
[187]F. Sanchez-Doblado, P. Andreo, R. Capote, A. Leal, M. Perucha, R. Arrans, L. Nunez, E. Mainegra, J. I. Lagares, and E. Carrasco, "Ionization chamber dosimetry of small photon fields: a Monte Carlo study on stopping-power ratios for radiosurgery and IMRT beams," Phys. Med. Biol. **48**, 2081–2099 (2003).

[188]R. Capote, F. Sanchez-Doblado, A. Leal, J. I. Lagares, R. Arrans, and G. H. Hartmann, "An EGSnrc Monte Carlo study of the microionization chamber for reference dosimetry of narrow irregular IMRT beamlets," Med. Phys. **31**, 2416–2422 (2004).
[189]P. Björk, T. Knöös, and P. Nilsson, "Measurements of output factors with different detector types and Monte Carlo calculations of stopping-power ratios for degraded electron beams," Phys. Med. Biol. **49**, 4493–4506 (2004).
[190]A. Wu, R. D. Zwicker, A. M. Kalend, and Z. Zheng, "Comments on dose measurements for a narrow beam in radiosurgery," Med. Phys. **20**, 777–779 (1993).
[191]J. Seuntjens and F. Verhaegen, "Comments on 'ionization chamber dosimetry of small photon fields: A Monte Carlo study on stopping-power ratios for radiosurgery and IMRT beams,'" Phys. Med. Biol. **48**, L43–L45 (2003).
[192]A. O. Jones and I. J. Das, "Comparison of inhomogeneity correction algorithms in small photon fields," Med. Phys. **32**, 766–776 (2005).
[193]M. Roach, M. DeSilvio, C. Lawton, V. Uhl, M. Machtay, M. J. Seider, M. Rotman, C. Jones, S. O. Asbell, R. K. Valicenti, S. Han, C. R. Thomas, and W. S. Shipley, "Phase III trial comparing whole=pelvic versus prostate-only radiotherapy and neoadjuvant versus adjuvant combined androgen suppression: Radiation therapy oncology group 9413," J. Clin. Oncol. **21**, 1904–1911 (2003).
[194]C. Martens, C. De Wagter, and W. De Neve, "The value of the PinPoint ion chamber for characterization of small field segments used in intensity-modulated radiotherapy," Phys. Med. Biol. **45**, 2519–2530 (2000).
[195]I. J. Das, M. B. Downes, A. Kassaee, and Z. Tochner, "Choice of radiation detector in dosimetry of stereotactic radiosurgery-radiotherapy," J. Radiosurg. **3**, 177–185 (2000).
[196]L. B. Leybovich, A. Sethi, and N. Dogan, "Comparison of ionization chambers of various volumes for IMRT absolute dose verification," Med. Phys. **30**, 119–123 (2003).
[197]J. W. Sohn, J. F. Dempsey, T. S. Suh, and D. A. Low, "Analysis of various beamlet sizes for IMRT with 6 MV photons," Med. Phys. **30**, 2432–2439 (2003).
[198]G. X. Ding, J. E. Cygler, and C. B. Kwok, "Clinical reference dosimetry: Comparison between AAPM TG-21 and TG-51 protocols," Med. Phys. **27**, 1217–1225 (2000).
[199]G. Ding, "Dose discrepancies between Monte Carlo calculations and measurements in the buildup region for a high-energy photon beam," Med. Phys. **29**, 2459–2463 (2002).
[200]F. Haryanto, M. Fippel, W. Laub, O. Dohm, and F. Nusslin, "Investigation of photon beam output factors for conformal radiation therapy-Monte Carlo simulations and measurements," Phys. Med. Biol. **47**, N133–N143 (2002).
[201]H. Bouchard and J. Seuntjens, "Ionization chamber-based reference dosimetry of intensity modulated radiation beams," Med. Phys. **31**, 2454–2465 (2004).
[202]F. F. Yin, J. Zhu, H. Yan, H. Gaun, R. Hammoud, S. Ryu, and J. H. Kim, "Dosimetric characteristics of Novalis shaped beam surgery unit," Med. Phys. **29**, 1729–1738 (2002).
[203]S. Li, A. Rashid, S. He, and D. Djajaputra, "A new approach in dose measurement and error analysis for narrow photon beams (beamlets) shaped by different multileaf collimators using a small detector," Med. Phys. **31**, 2020–2032 (2004).
[204]D. S. Followill, D. S. Davis, and G. S. Ibbott, "Comparison of electron beam characteristics from multiple accelerators," Int. J. Radiat. Oncol., Biol., Phys. **59**, 905–910 (2004).
[205]ICRU 35, *Radiation Dosimetry: Electron Beams with Energies Between* 1 to 50 MeV, ICRU Report 35 (International Commission on Radiation Units and Measurements, Bethesda, MD, 1984).
[206]T. C. Zhu, I. J. Das, and B. E. Bjärngard, "Characteristics of bremsstrahlung in electron beams," Med. Phys. **28**, 1352–1358 (2001).
[207]M. D. Mills, K. R. Hogstrom, and P. R. Almond, "Prediction of electron beam output factors," Med. Phys. **9**, 60–68 (1982).
[208]P. A. Jursinic and T. R. Mackie, "Characteristics of secondary electrons produced by 6, 10, and 24 MV x-ray beams," Phys. Med. Biol. **41**, 1499–1509 (1996).
[209]F. M. Khan, P. D. Higgins, B. J. Gerbi, F. C. Deibel, A. Sethi, and D. N. Mihailidis, "Calculation of depth dose and dose per monitor unit for irregularly shaped electron fields," Phys. Med. Biol. **43**, 2741–2754 (1998).
[210]C. M. Ma, B. A. Faddegon, D. W. Rogers, and T. R. Mackie, "Accurate characterization of Monte Carlo calculated electron beams for radiotherapy," Med. Phys. **24**, 401–416 (1997).
[211]L. J. van Battum and H. Huizenga, "On the initial angular variances of clinical electron beams," Phys. Med. Biol. **44**, 2803–2820 (1999).
[212]E. R. Cecatti, J. F. Goncalves, S. G. P. Cecatti, and M. P. Silva, "Effect of the accelerator design on the position of the effective electron source," Med. Phys. **10**, 683–686 (1983).
[213]A. Jamshidi, F. T. Kuchnir, and C. S. Reft, "Determination of the source position for the electron beams from a high-energy linear accelerator," Med. Phys. **13**, 942–948 (1986).
[214]K. Y. Quach, M. J. Butson, and P. E. Metcalfe, "Comparison of effective source-surface distances for electron beams derived from measurements made under different scatter conditions," Australas. Phys. Eng. Sci. Med. **22**, 99–102 (1999).
[215]D. M. Roback, F. M. Khan, J. P. Gibbons, and A. Sethi, "Effective SSD for electron beams as a function of energy and beam collimation," Med. Phys. **22**, 2093–2095 (1995).
[216]F. M. Khan, W. Sewchand, and S. H. Levitt, "Effect of air space on depth dose in electron beam therapy," Radiother. Oncol. **126**, 249–251 (1978).
[217]L. J. van Battum and H. Huizenga, "Film dosimetry of clinical electron beams," Int. J. Radiat. Oncol., Biol., Phys. **18**, 69–76 (1990).
[218]C. M. Ma and S. B. Jiang, "Monte Carlo modeling of electron beams from medical accelerators," Phys. Med. Biol. **44**, R157–R189 (1999).
[219]S. B. Jiang, A. Kapur, and C. M. Ma, "Electron beam modeling and commissioning for Monte Carlo treatment planning," Med. Phys. **27**, 180–191 (2000).
[220]A. Kapur, C. M. Ma, E. C. Mok, D. O. Findley, and A. L. Boyer, "Monte Carlo calculations of electron beam output factors for a medical linear accelerator," Phys. Med. Biol. **43**, 3479–3494 (1998).
[221]J. A. Antolak, M. R. Bieda, and K. R. Hogstrom, "Using Monte Carlo methods to commission electron beams: A feasibility study," Med. Phys. **29**, 771–786 (2002).
[222]J. E. Cygler, G. M. Daskalov, G. H. Chan, and G. X. Ding, "Evaluation of the first commercial Monte Carlo dose calculation engine for electron beam treatment planning," Med. Phys. **31**, 142–153 (2004).
[223]G. X. Ding, D. M. Duggan, C. W. Coffey, P. Shokrani, and J. E. Cygler, "First macro Monte Carlo based commercial dose calculation module for electron beam treatment planning—New issues for clinical consideration," Phys. Med. Biol. **51**, 2781–2799 (2006).
[224]R. A. Popple, R. Weinber, J. A. Antolak, S. J. Ye, P. N. Pareek, J. Duan, S. Shen, and I. A. Brezovich, "Comprehensive evaluation of a commercial macro Monte Carlo electron dose calculation implementation using a standard verification data set," Med. Phys. **33**, 1540–1551 (2006).
[225]M. Udale Smith, "Monte Carlo calculations of electron beam parameters for three Philips linear accelerators," Phys. Med. Biol. **37**, 85–105 (1992).
[226]J. Sempau, A. Sánchez-Reyes, F. Salvat, H. Oulad ben Tahar, S. B. Jiang, and J. M. Fernández-Varea, "Monte Carlo simulation of electron beams from an accelerator head using PENELOPE," Phys. Med. Biol. **46**, 1163–1186 (2001).
[227]P. R. Bevington, *Data Reduction and Error Analysis for the Physical Sciences* (McGraw-Hill, New York, 1969).
[228]W. H. Press, S. A. Teukolsky, W. T. Vetterling, and B. P. Flannery, *Numerical Recipes in C: The Art of Scientific Computing* (Cambridge University Press, New York, 1992).
[229]MATLAB documentation version 7.2.0.232 The Mathworks, Natick, MA, 2006.
[230]www.rpdinc.com.